

Strategy for mitigating wake interference between offshore vertical-axis wind turbines: Evaluation of vertically staggered arrangement

Limin Kuang^{a,b}, Hiroshi Katsuchi^b, Dai Zhou^{a,c,d,*}, Yaoran Chen^e, Zhaolong Han^{a,c}, Kai Zhang^{a,c}, Jiaqi Wang^b, Yan Bao^{a,c}, Yong Cao^{a,c}, Yijie Liu^f

^a School of Naval Architecture, Ocean and Civil Engineering, Shanghai Jiao Tong University, Shanghai 200240, China

^b Department of Civil Engineering, Yokohama National University, Yokohama 240-8501, Japan

^c State Key Laboratory of Ocean Engineering, Shanghai Jiao Tong University, Shanghai 200240, China

^d Key Laboratory of Hydrodynamics of Ministry of Education, Shanghai Jiao Tong University, Shanghai 200240, China

^e School of Artificial Intelligence, Shanghai University, Shanghai 200444, China

^f Department of Mechanical Engineering, The University of Tokyo, Tokyo 113-8654, Japan

HIGHLIGHTS

- Wake interference between two staggered offshore MW-class VAWTs is investigated.
- Knowledge of how vertically staggered arrangement affects wake interference is enriched.
- Effectiveness of horizontally and vertically staggered arrangements is compared.
- Relatively optimal layout of the turbine array is identified based on the Taguchi method.
- Findings would contribute to the layout design of offshore wind farms.

ARTICLE INFO

Keywords:

Offshore VAWTs
Vertically staggered arrangement
Wake interference
Power output
Taguchi method

ABSTRACT

Wake interference between wind turbines potentially decreases the power output of offshore wind farms. While the staggered arrangement shows promise for mitigating this interference, the understanding of the impact of vertically staggered setup remains ambiguous, especially in the case of vertical-axis wind turbines (VAWTs). Also, the difference between horizontally and vertically staggered arrangements needs to be clarified. This study aims to shed light on these ambiguities, systematically evaluating the effectiveness of vertically staggered arrangement in mitigating wake interference between offshore VAWTs. High-fidelity computational fluid dynamics simulations are used to investigate the wake interference between two vertically staggered MW-class VAWTs. Typical separation distances ($3D \leq L_S \leq 7D$) and different vertically staggered distances ($-0.25H \leq L_V \leq 0.75H$) are considered, where D and H denote the turbine diameter and blade span length, respectively. Employing the Taguchi method, the effectiveness of horizontally and vertically staggered arrangements is compared, and the relatively optimal layout of the turbine array is identified. The results show that the vertically staggered arrangement significantly improves the power performance of the downstream turbine, e.g., the power output increases by 75.96% when $L_S = 7D$ and $L_V = 0.25H$. When dealing with smaller L_S (e.g., $3D$), a negative L_V is suggested, which reduces the tower cost while preserving the performance improvement. The vertically staggered arrangement has a greater impact on wake interference than the horizontally staggered arrangement. In terms of the relatively optimal layout, the power output of the turbine array is increased by 46.27%. These findings would contribute to the layout design of offshore wind farms.

* Corresponding author at: School of Naval Architecture, Ocean and Civil Engineering, Shanghai Jiao Tong University, Shanghai 200240, China.
E-mail address: zhoudai@sjtu.edu.cn (D. Zhou).

1. Introduction

An uptick in global energy demand, coupled with the environmental implications of traditional fossil fuels, underscores the urgency for clean and sustainable alternatives [1]. Wind energy emerges as a promising response to this call [2]. Offshore wind energy exploitation is garnering considerable traction, leading to a rise in offshore wind farm deployments [3,4]. Wind turbines, divisible into two types—horizontal-axis wind turbines (HAWTs) and vertical-axis wind turbines (VAWTs)—form the backbone of these farms [5,6]. Historically, HAWTs have enjoyed commercial supremacy due to their robust performance and technology maturity [7,8]. However, VAWTs are now receiving recognition as prospective contenders. Their allure lies in several unique advantages, including omnidirectionality, design simplicity, scalability, and potential for high space efficiency [2,9]. Also, the typically poor power performance of small-scale VAWTs is not applicable to MW-class VAWTs due to the Reynolds number effect [10,11]. Hence, fundamental research on offshore wind farms consisting of VAWTs is warranted.

Wake interference is a significant concern in offshore wind farms. The wake effects of upstream turbines, including velocity deficit and turbulence, can lead to substantial changes in the aerodynamics of downstream ones, which may decrease the power output of wind farms [12,13]. Evidence of this can be found in examples such as the Horns Rev wind farm, where the power loss of downstream turbines reached 40% in the prevailing wind direction [14]. More compact wind farms, like Lillgrund, may experience even harsher conditions [15]. This scenario underscores the necessity of investigating wake interference and formulating strategies to mitigate its negative impact.

Since the wake of upstream turbines fundamentally drives wake interference, numerous studies have been conducted to characterize the impact of operational and geometrical parameters on the wake characteristics of stand-alone VAWTs. These parameters include turbulence intensity (TI) [16], tip speed ratio (TSR) [17], Reynolds number [10], platform motion [18], rotor solidity [19], and blade aspect ratio [20]. Research in these areas lays the foundation for further investigation of wake interference. Accordingly, numerical studies have been extensively conducted to better understand this phenomenon. Zuo et al. [21] analyzed the wake interference between two aligned scaled VAWTs with different separation distances using computational fluid dynamics (CFD) simulations. They found that the power coefficient of the downstream VAWT increased linearly with increasing separation distance. Kuang et al. [22] confirmed this finding and further concluded that a higher TI would reduce the wake interference between VAWTs. Also, Kuang et al. [23] numerically characterized the wake interference between two aligned scaled floating VAWTs. The results showed that placing the downstream VAWT in the moderate wake region of the upstream one could properly balance the space cost and power output of the turbine array. Experiments by Kinzel et al. [24], Ahmadi-Baloutaki et al. [25], and Su et al. [26] support these results and provide insightful suggestions for the layout design of offshore wind farms.

Benefiting from the above fundamental research, the investigation of strategies for mitigating the negative impact of wake interference has reached a fairly comprehensive level. Driven by the field tests of Dabiri [27], the concept of closely spaced arrangement has become a focus in recent years. This strategy utilizes the increased velocity between closely spaced VAWTs to improve the turbine performance [28]. While

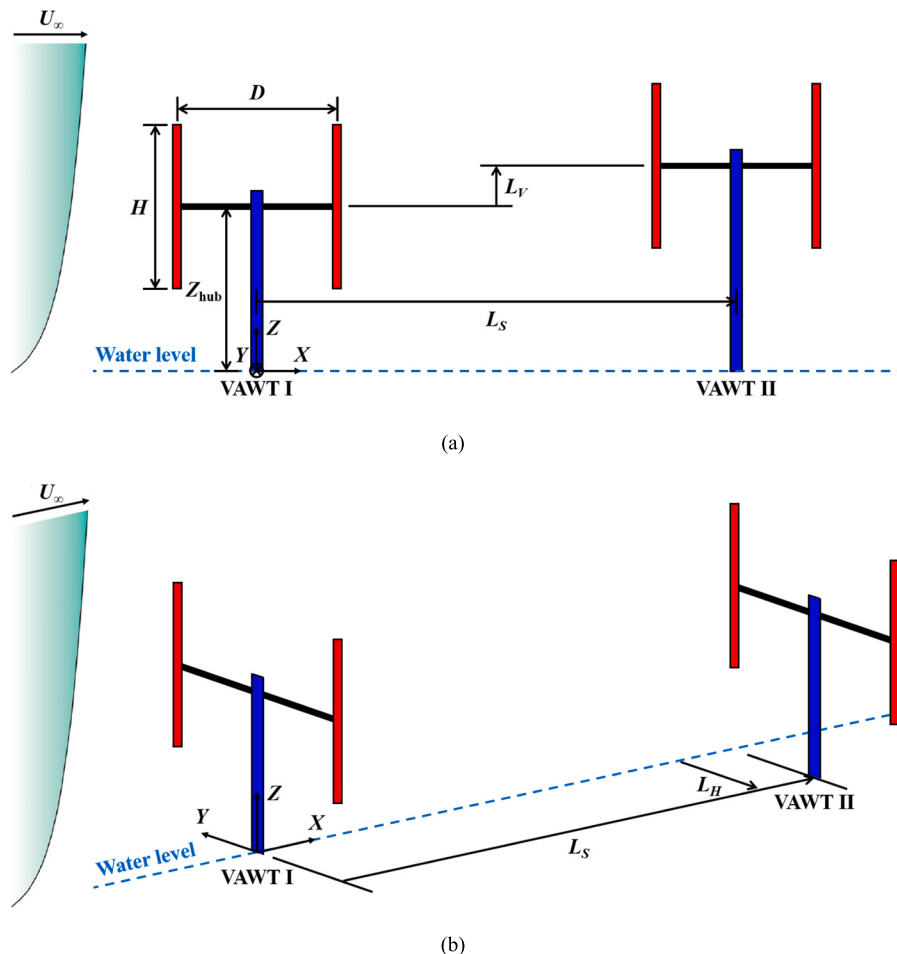


Fig. 1. Schematic of two staggered offshore VAWTs: (a) vertically staggered; (b) horizontally staggered.

analyzing the aerodynamic mechanisms, researchers also considered various operational and geometrical parameters for layout optimization, such as rotational direction [29], phase lag [30], rotor solidity [31], and blade pitch angle [32]. However, due to potential safety concerns and technical limitations of closely spaced arrangement, an alternative strategy of staggered arrangement with relatively large separation distances (over three times the turbine diameter), may be more feasible.

There are two main types of staggered arrangements, i.e., horizontally and vertically. The horizontally staggered arrangement is the conventional strategy for mitigating wake interference and the main approach for optimizing the layout of offshore wind farms. Its effectiveness has been evaluated by numerous studies [33–36]. On the contrary, the vertically staggered arrangement has been somewhat overlooked. Studies focusing on wake interference between vertically staggered VAWTs are scant, leaving the understanding of how this arrangement affects wake interference ambiguous. The task of evaluating its effectiveness in mitigating wake interference is still largely unfulfilled. While numerical studies on HAWTs have been conducted [37–40], their scientific significance and engineering feasibility remain questionable. Given the near-axisymmetric turbine geometry, the wake patterns of HAWTs are almost identical in the horizontal and vertical planes. This similarity leads to comparable impacts of horizontally and vertically staggered arrangements on wake interference, thus diminishing the scientific significance. Also, the vertically staggered arrangement raises the hub height of wind turbines, potentially causing structural issues with the turbine towers and increasing manufacturing costs, thereby reducing the engineering feasibility. However, the research on vertically staggered VAWTs is sufficiently motivated by the following factors:

- Compared to the horizontally staggered arrangement, the vertically staggered arrangement can take advantage of the higher wind speeds associated with the increased hub height to further improve turbine performance. Also, it does not occupy the sea area of wind farms, which helps to increase the power density.
- Unlike HAWTs, VAWTs have different wake patterns in the horizontal and vertical planes. Therefore, the impact of horizontally and vertically staggered arrangements on wake interference should be different, which deserves further investigation.
- With the evolution of turbine tower manufacturing technology, commercial wind turbines can now reach hub heights of at least 150 m [41], and the wooden modular towers designed by Modvion can reach hub heights of 290 m [42]. These developments greatly enhance the engineering feasibility of vertically staggered arrangement.

Given these motivations, this study aims to:

- Use high-fidelity CFD simulations to investigate the wake interference between vertically staggered offshore VAWTs. The layout of two tandem MW-class VAWTs is considered, which is the most basic and representative.
- Employ the Taguchi method to compare the impact of horizontally and vertically staggered arrangements on wake interference and identify the relatively optimal turbine array layout.
- In addition to power performance, analyze the dynamic loads, wake profiles, and flow structures of VAWTs to better understand the aerodynamic mechanisms.

The novelty of this study lies in its first-time evaluation of the effectiveness of vertically staggered arrangement in mitigating wake interference between offshore MW-class VAWTs. The main contributions include: (1) The knowledge of how vertically staggered arrangement affects wake interference between VAWTs is enriched. (2) The feasibility of horizontally and vertically staggered arrangements in increasing the power output of VAWT arrays is characterized. These

Table 1
Properties of the VAWT.

Property	Value
Blade number N	2
Turbine diameter D	78 m
Blade span length H	80 m
Blade chord length c	4.05 m
Hub height Z_{hub}	79.78 m
Blade section	NACA0018
Rated wind speed U_{hub}	14 m/s

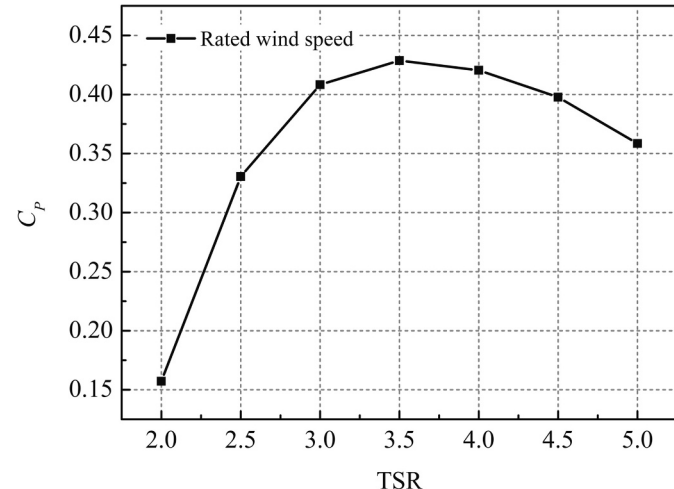


Fig. 2. Mean power coefficients C_p of the VAWT for different TSRs at the rated wind speed. ($\text{TSR} = \omega D / 2U_{\text{hub}}$, $C_p = Q\omega / 0.5\rho U_{\text{hub}}^3 HD$, where Q , ω , and ρ denote the torque, rotational speed, and air density, respectively).

insights could inform the layout design of offshore wind farms.

The remaining sections are structured as follows: Section 2 elaborates on the properties of offshore VAWTs. Section 3 outlines the numerical model. Section 4 and 5 discuss the evaluation of vertically staggered arrangement. Section 6 concludes with a summary.

2. Turbine model

Fig. 1 shows a schematic of two staggered offshore VAWTs. L_S , L_V , and L_H denote the separation distance, vertically staggered distance, and horizontally staggered distance between the upstream turbine (VAWT I) and the downstream turbine (VAWT II), respectively. A conceptual MW-class offshore VAWT designed by the Norwegian University of Science and Technology [43] is selected as the turbine model. This VAWT is widely used in dynamic response analyses due to its good design and performance [44,45]. The properties of the VAWT are listed in Table 1. The shafts and struts are not considered in the numerical modeling as they have a small impact on turbine aerodynamics [5]. Fig. 2 shows the mean power coefficients C_p of the VAWT for different TSRs at the rated wind speed. The maximum power coefficient, $C_{p,\max} = 0.4287$, is achieved at $\text{TSR} = 3.5$ (rotational speed of 12 rpm), corresponding to a maximum power output of $P_{\max} = 4.5 \text{ MW}$.

3. Numerical model

Transient simulations are conducted using the commercial software STAR-CCM+ (version 13.04) [46]. The shear stress transport (SST) $k-\omega$ model is employed for turbulence modeling. This model is well-regarded for its accuracy in simulating the aerodynamics of small-scale VAWTs [47,48]. Also, it has been extensively employed to simulate MW-class HAWTs [49,50], which demonstrates its reliability in handling high Reynolds number flow problems. In addition, compared to scale-

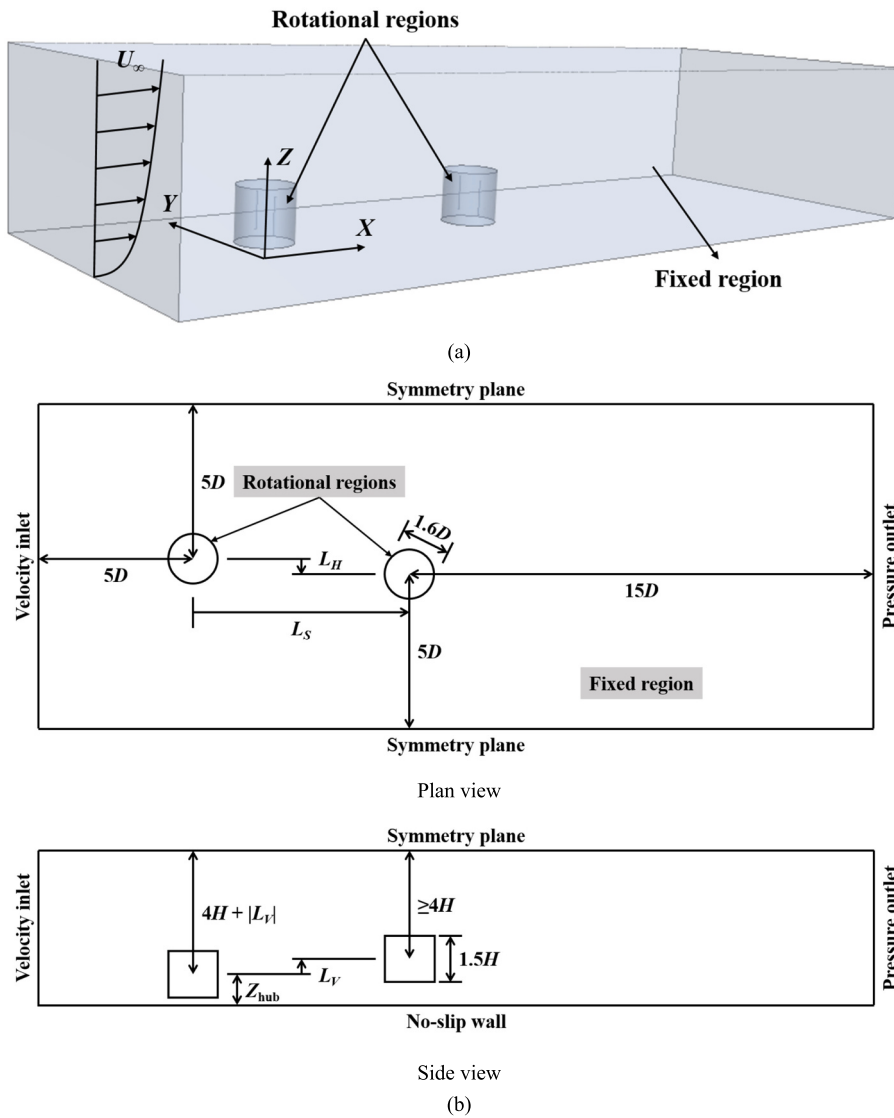


Fig. 3. Computational domain: (a) three-dimensional view for the case of aligned arrangement ($L_S = 7D$, $L_V = 0$, $L_H = 0$); (b) plan and side views for the case of combined staggered arrangement ($L_S = 7D$, $L_V \neq 0$, $L_H \neq 0$).

resolving methods such as large-eddy simulation (LES), the Reynolds-Averaged Navier-Stokes (RANS) method can provide a good balance between accuracy and cost [51].

When performing CFD simulations of wind turbines, STAR-CCM+, ANSYS Fluent (both commercial software), and OpenFOAM (an open-source software) are commonly used. STAR-CCM+ stands out for its streamlined user interface, robust pre- and post-processing tools (STAR-CCM+ seamlessly integrates geometry modeling and meshing modules, whereas ANSYS Fluent relies on external tools such as SpaceClaim), and sophisticated overset mesh and volume of fluid techniques (ideal for modeling floating wind turbines [52]). ANSYS Fluent features a range of

advanced numerical methods, such as scale-adaptive simulation [53], and its powerful user-defined functions enable more convenient modifications of numerical settings like boundary conditions [54]. ANSYS Fluent also provides a comprehensive user guide and extensive tutorial resources for user support. OpenFOAM, on the other hand, offers a free platform for integrating the latest numerical methods, addressing the limitations of proprietary software codes. Notably, its actuator disc and actuator line models allow researchers to simulate turbine aerodynamics with reasonable accuracy and lower cost [55]. Solvers such as turbinesFoam are frequently employed for the layout design of offshore wind farms [55,56]. However, the learning curve and usage complexity of OpenFOAM are higher than those of STAR-CCM+ and ANSYS Fluent. Overall, the selection of simulation software should align with the research objectives and numerical methods.

Table 2
Details of the boundary conditions.

Region	Boundary	Specification
Fixed region	Inlet	Velocity inlet, $U_\infty = U_{\text{hub}}(Z/Z_{\text{hub}})^{0.14}$ Turbulence intensity of 1%
	Outlet	Pressure outlet, gauge pressure of 0 Pa
	Top and sides	Symmetry plane
Rotational region	Bottom	No-slip wall
	Cylindrical surface	Interface
	Turbine surface	No-slip wall

3.1. Computational domain and mesh topology

As shown in Fig. 3, the computational domain comprises a rectangular fixed region and two cylindrical rotational regions. The information exchange between these regions is realized through sliding mesh technique. The VAWTs are placed in the rotational regions and can

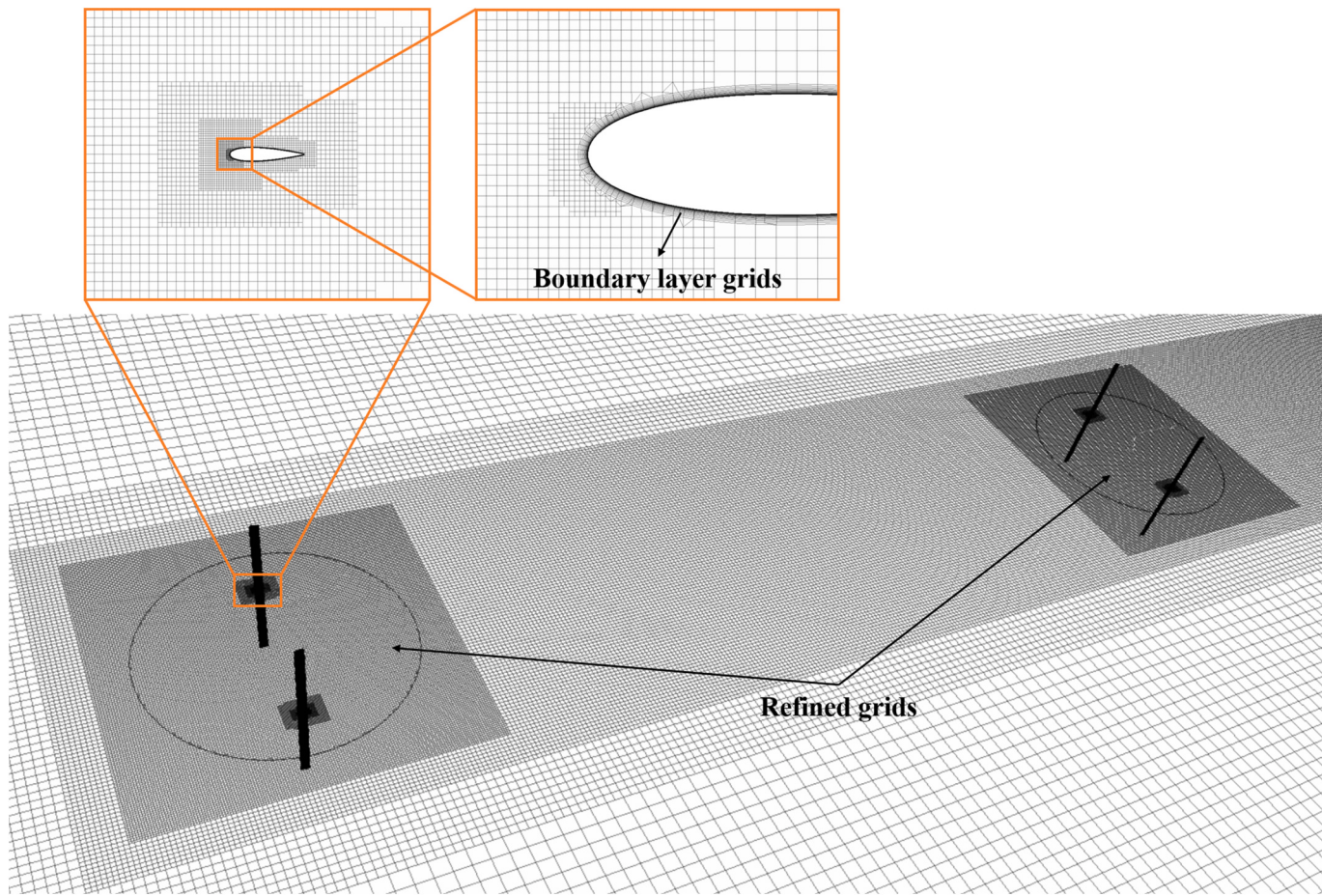


Fig. 4. Mesh topology for the case of aligned arrangement. ($L_S = 7D$, $L_V = 0$, $L_H = 0$).

rotate at a prescribed speed. The dimension of the domain is selected based on the authors' previous studies [22,23]. The length, width, and height of the fixed region are $20D + L_S$, $10D + |L_H|$, and $Z_{\text{hub}} + 4H + |L_V|$, respectively. The height and diameter of the rotational regions are $1.5H$ and $1.6D$, respectively.

Table 2 lists the details of the boundary conditions. A shear wind condition is specified at the inlet of the fixed region, which is consistent with the normal wind profile employed in the study of Cheng et al. [43]. The power law exponent is selected as 0.14 in accordance with the IEC 61400-3-1 standard for offshore wind turbines [57]. Note that a turbulence intensity of 1% is considered, which is lower than the actual operating conditions of wind turbines. Nevertheless, given the aim of this study—to evaluate the effectiveness of vertically staggered arrangement in mitigating wake interference between VAWTs—the main conclusions remain valid. Also, this setting simplifies numerical modeling and reduces computational cost. The impact of turbulence intensity on VAWT arrays was characterized in the authors' previous study [22].

Fig. 4 shows the mesh topology for the case of aligned arrangement ($L_S = 7D$, $L_V = 0$, $L_H = 0$). Grids around the VAWTs are refined. Boundary layer grids are distributed around the VAWTs to accurately simulate the viscous sublayer flows. The number of layers, thickness, and growth rate of the boundary layer grids are 44, 0.06 m, and 1.2, respectively. This arrangement ensures the maximum y^+ of the blades remains below 1 during the simulations. For the case of aligned arrangement, the total number of grids is 43.8 million. The mesh independence test is provided in Supplementary material S.1.

Table 3
Solver settings.

Flow solver	Segregated	
Pressure-velocity coupling scheme	SIMPLE	
Discretization scheme	Time	2nd order
	Convection	2nd order upwind
Time step	$T/360$ (T denotes the time for one turbine revolution)	
Inner iteration	20	

3.2. Solver settings

Solver settings listed in Table 3 are selected based on the authors' previous studies [48,58] and also with reference to the CFD guidelines for VAWTs [59] and the transient simulation guidelines in STAR-CCM+ [46]. The detailed simulation setup can be found in Supplementary material S.2. Also, the time step independence test and the validation of the numerical model are provided in Supplementary material S.3 and S.4, respectively. It should be noted that the aerodynamic parameters of VAWTs are counted when the mean values of two consecutive turbine revolutions vary by $<0.1\%$ [60].

4. Wake interference between vertically staggered turbines

This section investigates the wake interference between two vertically staggered VAWTs, aiming to evaluate the effectiveness of vertically staggered arrangement in mitigating wake interference. Two typical separation distances of $L_S = 3D$ and $7D$ are considered, corresponding to

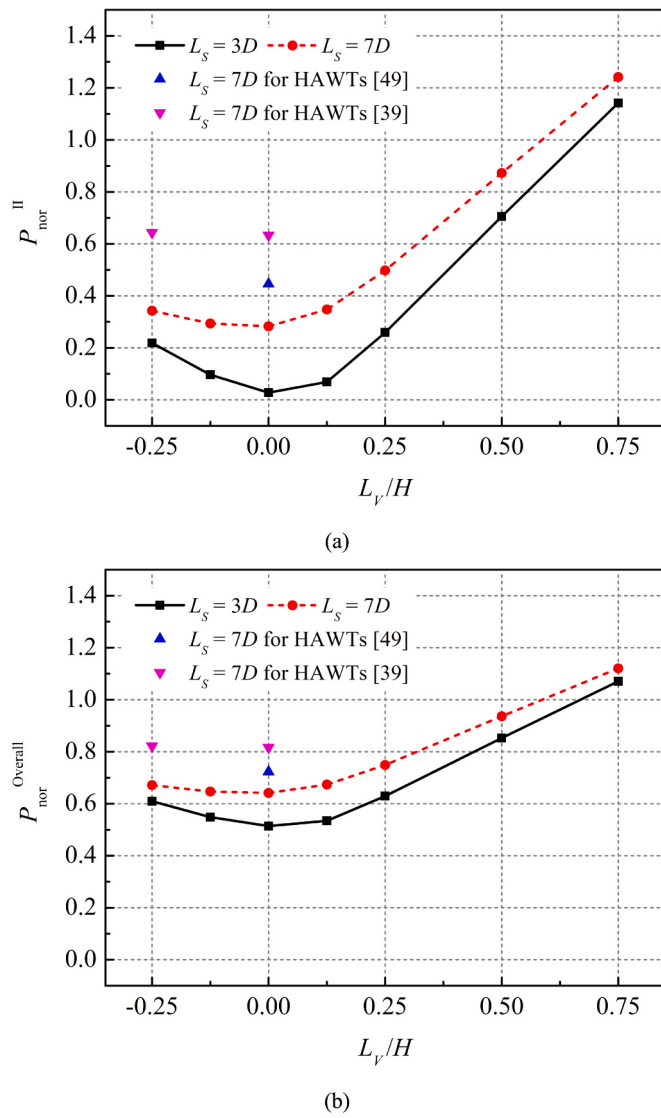


Fig. 5. Mean $P_{\text{nor}}^{\text{II}}$ and $P_{\text{nor}}^{\text{Overall}}$ for different L_s and L_v : (a) $P_{\text{nor}}^{\text{II}}$; (b) $P_{\text{nor}}^{\text{Overall}}$.

the turbine spacings of the Lillgrund [15] and Horns Rev [14] wind farms, respectively. Assuming a constant hub height of 79.78 m for VAWT I, six vertically staggered distances of $L_v = \pm 0.125H, \pm 0.25H, 0.5H$, and $0.75H$ are selected for VAWT II. The case of aligned arrangement ($L_v = 0$) is also included for comparison. The selection of L_v is guided by the studies of Zhang et al. [38] and Wu et al. [39,61], where the hub heights of MW-class wind turbines ranged from 60 m to 150 m. Both VAWTs operate at a rotational speed of 12 rpm, which matches the optimal TSR of the stand-alone VAWT. Note that in an actual wind farm, the wind turbine will control its rotational speed according to the inflow conditions to maintain a stable and sufficient power output [62]. However, due to the immature control strategy of the selected VAWT and to simplify the modeling and analysis procedures, the rotational speed of the downstream turbine is set the same as that of the upstream one, which is a common practice for studying VAWT arrays [21,30,63,64].

4.1. Power performance and dynamic load analysis

Fig. 5 shows the mean $P_{\text{nor}}^{\text{II}}$ and $P_{\text{nor}}^{\text{Overall}}$ for different L_s and L_v . $P_{\text{nor}}^{\text{II}}$ is the power output of VAWT II normalized by the mean power output of the stand-alone VAWT (P_{max} , refer to Section 2). $P_{\text{nor}}^{\text{Overall}}$ is the normalized power output of the turbine array, calculated as the arithmetic

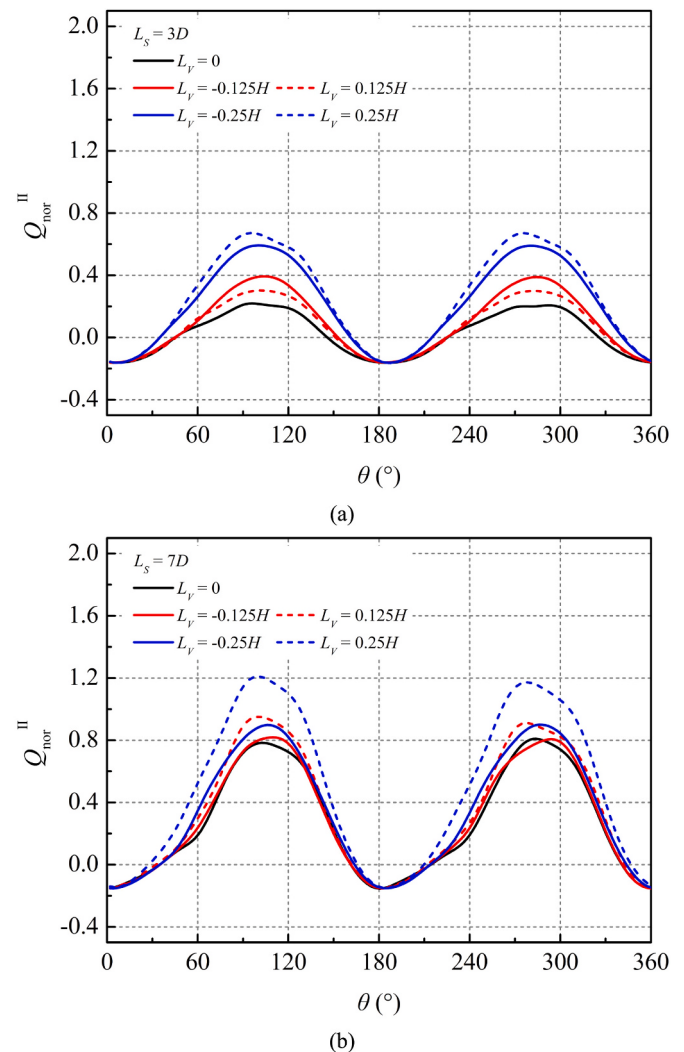


Fig. 6. Instantaneous $Q_{\text{nor}}^{\text{II}}$ for different L_s and L_v : (a) $L_s = 3D$; (b) $L_s = 7D$. (θ denotes the azimuthal angle).

mean of $P_{\text{nor}}^{\text{I}}$ and $P_{\text{nor}}^{\text{II}}$. The results of Miao et al. [49] and Wu et al. [39] for HAWTs are included for comparison. Note that in the study of Wu et al. [39], inflow turbulence and wind turbine control strategy were considered, resulting in a relatively high power output of the downstream turbine. It can be observed that the power performance of VAWT II improves significantly in the case of vertically staggered arrangement. For example, when $L_v = 0.125H$, the $P_{\text{nor}}^{\text{II}}$ increases by 146.96% and 22.83% for $L_s = 3D$ and $7D$, respectively. The power performance of the turbine array also improves, with relative increases of 3.99% and 5.02% in $P_{\text{nor}}^{\text{Overall}}$ for $L_s = 3D$ and $7D$, respectively. Note that when the two VAWTs are aligned ($L_v = 0$), VAWT II experiences a significant velocity deficit, hence even a minor L_v can lead to considerable performance improvement. Also, the $P_{\text{nor}}^{\text{II}}$ and $P_{\text{nor}}^{\text{Overall}}$ for $L_s = 7D$ are higher than those for $L_s = 3D$ due to the wake recovery of VAWT I. In addition, it is found that the $P_{\text{nor}}^{\text{II}}$ and $P_{\text{nor}}^{\text{Overall}}$ increase linearly with increasing L_v when $L_v \geq 0.125H$ and exceed 1 when $L_v = 0.75H$. On the one hand, with the increase of L_v , VAWT II can avoid more wake interference and obtain a higher inflow velocity. On the other hand, this is a result of the velocity-height relationship in shear wind conditions. Therefore, it is expected that the $P_{\text{nor}}^{\text{II}}$ and $P_{\text{nor}}^{\text{Overall}}$ for positive L_v will be higher than those for negative one. However, when $L_s = 3D$, lower $P_{\text{nor}}^{\text{II}}$ and $P_{\text{nor}}^{\text{Overall}}$ are observed for $L_v = -0.125H$ than for $L_v = 0.125H$, which does not occur when $L_s = 7D$. The explanation of this unexpected phenomenon will be provided in the wake profile analysis. Moreover, the power performance

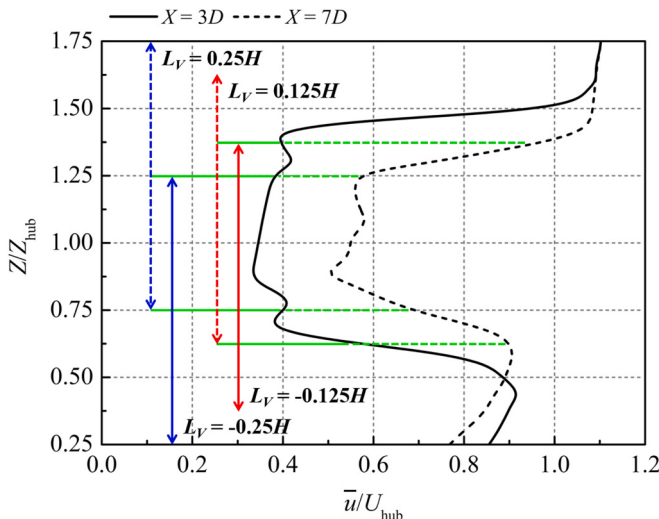


Fig. 7. Normalized mean wake profiles of VAWT I in the vertical plane ($Y = 0$) for different downstream distances. (u denotes the streamwise velocity. Dashed and solid vertical lines indicate the ranges of wake profiles experienced by VAWT II for positive and negative L_V , respectively, with different colors representing different absolute values of L_V . Green horizontal lines delineate the identical wake profiles experienced by VAWT II for positive and negative L_V). (For interpretation of the references to colour in this figure legend, the reader is referred to the web version of this article.)

of the VAWT array is found to be inferior to that of the HAWT array, implying stronger wake interference. This is mainly due to the slow wake recovery of the selected VAWT, which may be a common drawback of existing conceptual MW-class VAWTs and will be further elaborated in the subsequent section.

Fig. 6 shows the instantaneous $Q_{\text{nor}}^{\text{II}}$ for different L_S and L_V . $Q_{\text{nor}}^{\text{II}}$ is the torque of VAWT II normalized by the mean torque of the stand-alone VAWT. It can be observed that the dynamic load of VAWT II increases significantly in the presence of L_V . As the vertically staggered arrangement allows the downstream turbine to avoid partial wake interference from the upstream one, VAWT II experiences a higher inflow velocity and therefore obtains a larger $Q_{\text{nor}}^{\text{II}}$, leading to the performance improvement shown in Fig. 5. Also, higher $Q_{\text{nor}}^{\text{II}}$ is observed for positive L_V than for negative one when $L_S = 7D$. However, when $L_S = 3D$, the $Q_{\text{nor}}^{\text{II}}$ for $L_V = -0.125H$ is found to be higher than that for $L_V = 0.125H$, which corresponds to the higher $P_{\text{nor}}^{\text{II}}$ and $P_{\text{nor}}^{\text{Overall}}$ shown in Fig. 5. Besides, the dynamic loads for positive and negative L_V are close when $L_S = 3D$, while the difference is significant when $L_S = 7D$, especially for the case of $L_V = \pm 0.25H$. This phenomenon corresponds to the variation of turbine performance shown in Fig. 5, where the $P_{\text{nor}}^{\text{II}}$ and $P_{\text{nor}}^{\text{Overall}}$ for $L_V = -0.25H$ and $0.25H$ are close when $L_S = 3D$, while the $P_{\text{nor}}^{\text{II}}$ and $P_{\text{nor}}^{\text{Overall}}$ for $L_V = -0.25H$ are significantly lower than those for $L_V = 0.25H$ when $L_S = 7D$. Therefore, for a relatively small L_S , a negative L_V is suggested, as it can reduce the tower cost while preserving the performance improvement; for a relatively large L_S , a positive L_V is suggested, as it can bring considerable performance improvement and compensate for the negative impact of increased hub height. The explanation for these phenomena will be provided in the wake profile analysis.

4.2. Wake profile analysis

Fig. 7 shows the normalized mean wake profiles of VAWT I in the vertical plane ($Y = 0$) for different downstream distances. It can be observed that in the near wake region ($X = 3D$), the turbine wake exhibits a significant velocity deficit, e.g., the wake velocity at $Z = Z_{\text{hub}}$ is only 0.35 of the inflow velocity. This is consistent with the velocity profiles measured by Peng et al. [65]. Such strong wake interference deteriorates the aerodynamics of VAWT II, leading to the low $P_{\text{nor}}^{\text{II}}$ and

$P_{\text{nor}}^{\text{Overall}}$ shown in Fig. 5, especially for the aligned arrangement. In the moderate wake region ($X = 7D$), as the turbine wake recovers, the wake interference acting on VAWT II diminishes. However, since the wake velocity at $Z = Z_{\text{hub}}$ only recovers to 0.55 of the inflow velocity, the $P_{\text{nor}}^{\text{II}}$ for $L_V = 0$ only reaches 0.2829. Taking the Horns Rev wind farm as a comparison, the second row of HAWTs is placed at $L_S = 7D$, and field tests and numerical simulations showed their normalized power output to be about 0.6 [14,39], which is significantly higher than the results of the present study. The main reason is that to achieve appreciable power performance, conceptual MW-class VAWTs are commonly designed to have low rotor solidity, like those designed by Borg et al. [66] and Hand et al. [67]. The low solidity characteristic leads to slow wake recovery [19,68], thereby deteriorating the power performance of the downstream turbine. Therefore, for basic two-turbine arrays with relatively large turbine spacing, VAWTs are inferior to HAWTs, and the high space efficiency of VAWTs may only be demonstrated in closely spaced arrangement.

Fig. 7 shows that VAWT II experiences different ranges of wake profiles for positive and negative L_V . Fig. 8 compares the mean wake profiles experienced by VAWT II for positive and negative L_V . The identical wake profiles delineated by the green horizontal lines are excluded from this comparison. It can be observed that for $|L_V| = 0.125H$, VAWT II experiences a higher inflow velocity for positive L_V when $L_S = 7D$. This is mainly attributed to the velocity-height relationship in shear wind conditions. However, when $L_S = 3D$, by comparing the mean streamwise velocity \bar{u} in the ranges of $Z = (0.5Z_{\text{hub}}, 0.625Z_{\text{hub}})$ and $(1.375Z_{\text{hub}}, 1.5Z_{\text{hub}})$, it is found that the wake profile for negative L_V shows higher velocity than that for positive L_V . This phenomenon was also reported in wind tunnel tests by Chamorro et al. [69] and Rolin et al. [70]. This is because in the near wake region there is a blockage effect between the turbine wake and the sea surface (wind tunnel bottom surface), which increases the wake velocity. Even though the \bar{u} in the range of $Z = (0.375Z_{\text{hub}}, 0.5Z_{\text{hub}})$ is lower than that in the range of $Z = (1.5Z_{\text{hub}}, 1.625Z_{\text{hub}})$, VAWT II can still achieve better power performance for negative L_V due to the relatively low power efficiency in the tip region of VAWTs, corresponding to the higher $P_{\text{nor}}^{\text{II}}$ and $Q_{\text{nor}}^{\text{II}}$ shown in Fig. 5 and Fig. 6. For $|L_V| = 0.25H$, similar to the case of $|L_V| = 0.125H$, VAWT II experiences a higher inflow velocity for positive L_V when $L_S = 7D$. But when $L_S = 3D$, the benefit of negative L_V is no longer pronounced and is offset by the low ambient flow velocity in the tip region, leading to lower $P_{\text{nor}}^{\text{II}}$ and $Q_{\text{nor}}^{\text{II}}$.

As described above, the vertically staggered arrangement can significantly improve the power performance of two tandem VAWTs. However, offshore wind farms are composed of multiple basic two-turbine arrays, and the vertically staggered arrangement may affect wind turbines further downstream. Therefore, it is crucial to investigate the impact of vertically staggered arrangement on the wake of the turbine array. Fig. 9 shows a schematic of multiple staggered offshore VAWTs. $L_{S,2}$ denotes the separation distance between VAWT II and VAWT III, and the hub height of VAWT III is the same as that of VAWT I. Fig. 10 compares the mean wake profiles experienced by VAWT III for different L_S , $L_{S,2}$, and L_V . The following observations are made:

- For $L_S = 3D$, the vertically staggered arrangement significantly reduces the velocity deficit in the very near wake region of VAWT II, allowing VAWT III to obtain a higher inflow velocity when $L_{S,2} = 1.5D$. However, as $L_{S,2}$ increases, the velocity deficit for $L_V = 0.25H$ and $0.5H$ is larger than that for $L_V = 0$, especially in the range of $Z = (1.125Z_{\text{hub}}, 1.5Z_{\text{hub}})$. This suggests that VAWT III could face stronger wake interference in the case of vertically staggered arrangement.
- For $L_S = 7D$, a similar phenomenon occurs. The velocity deficit in the very near wake region of VAWT II is reduced when $L_V = 0.5H$. As $L_{S,2}$ increases, the velocity deficit in the range of $Z = (1.125Z_{\text{hub}}, 1.5Z_{\text{hub}})$ increases significantly in the case of vertically staggered arrangement.

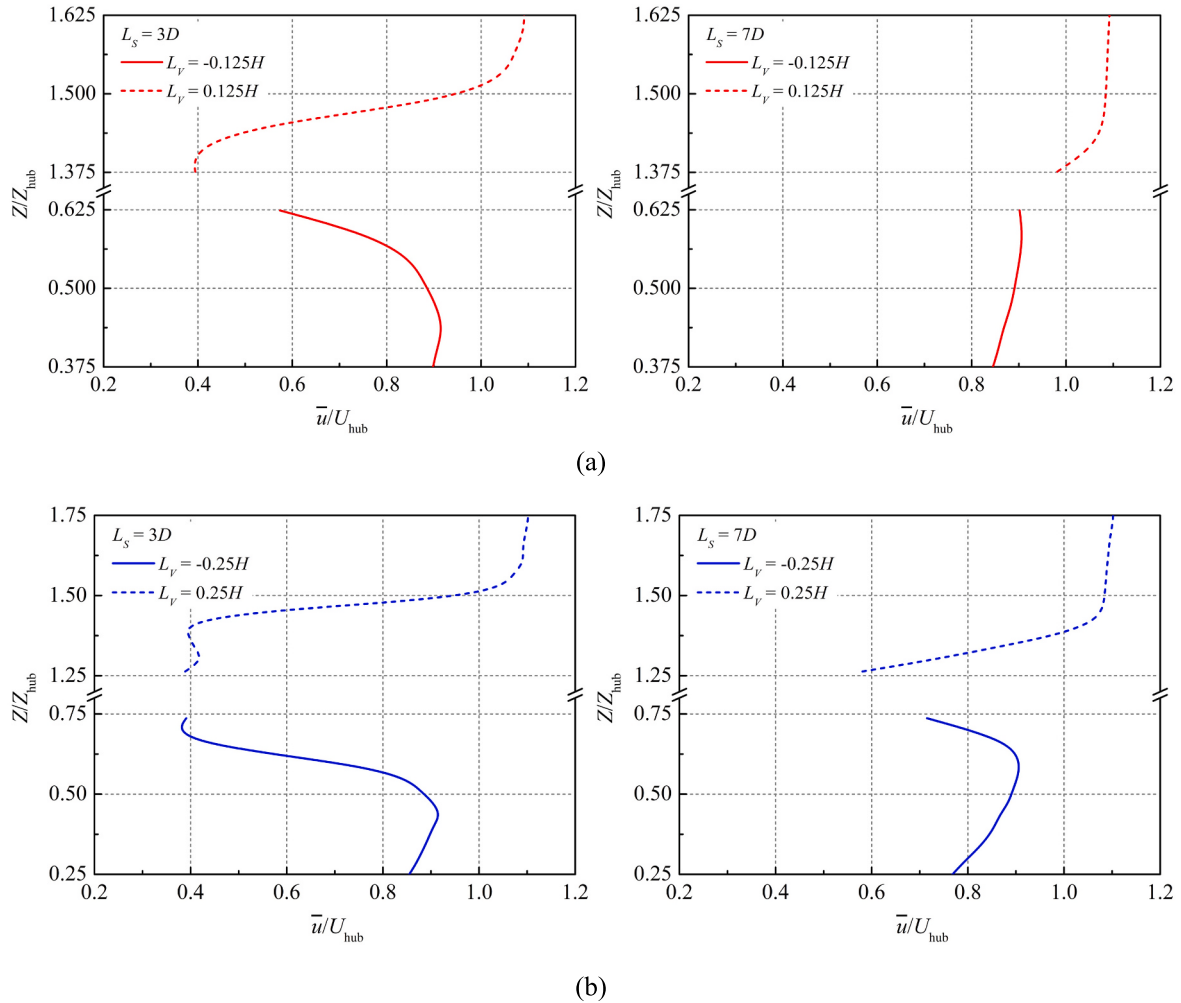


Fig. 8. Comparison of mean wake profiles experienced by VAWT II for positive and negative L_V : (a) $|L_V| = 0.125H$; (b) $|L_V| = 0.25H$.

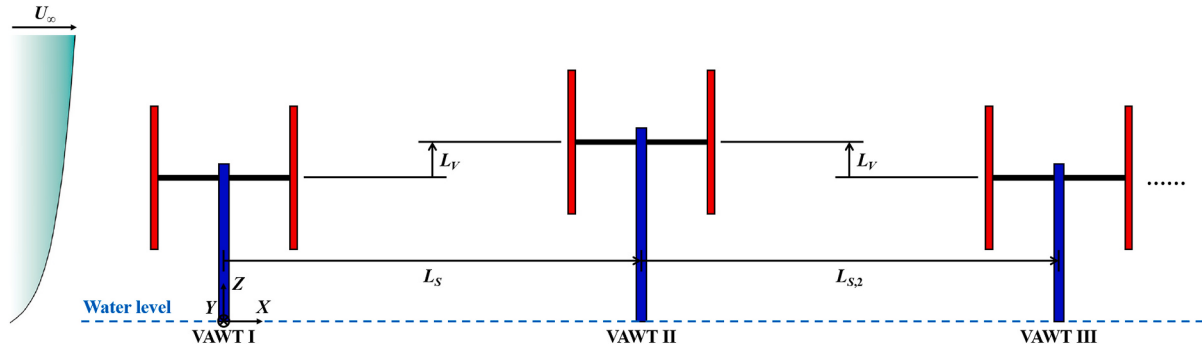


Fig. 9. Schematic of multiple vertically staggered offshore VAWTs.

- On the one hand, the vertically staggered arrangement potentially increases the power density of the turbine array as VAWT III can be placed more closely behind VAWT II. On the other hand, VAWT III faces a negative impact from the vertically staggered arrangement when it is placed in the moderate and far wake regions of VAWT II.

4.3. Flow structure analysis

Fig. 11 shows the instantaneous velocity distribution around the turbine array in the vertical plane ($Y = 0$) for different L_S and L_V . It can be observed that in the case of vertically staggered arrangement, VAWT

II can avoid partial wake interference and obtain a higher inflow velocity. When the two VAWTs are aligned, a significant velocity deficit appears in the very near wake region of VAWT II, corresponding to the low \bar{u} shown in Fig. 10. Also, as the wake of VAWT I fully acts on VAWT II and overlaps with that of VAWT II, the turbulence level in the turbine wake increases, promoting momentum exchange between the ambient flow and the wake and speeding up wake recovery. However, when $L_V = 0.25H$ and $0.5H$, the wake of VAWT II is less affected by VAWT I and gradually merges with the wake of VAWT I. This significantly slows the wake recovery and extends the wake boundary, which is expected to increase the range of velocity deficit experienced by VAWT III (refer to

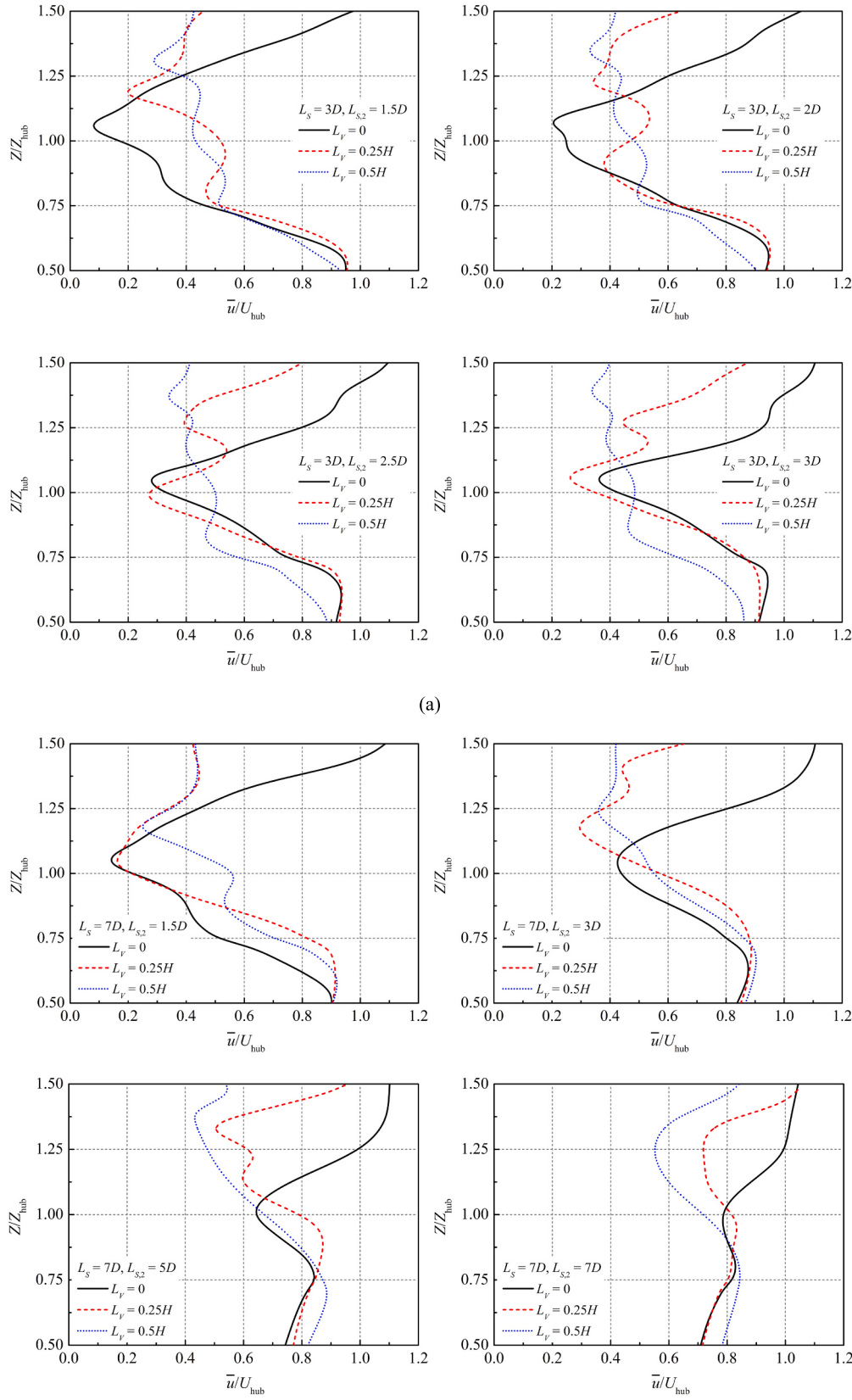


Fig. 10. Comparison of mean wake profiles experienced by VAWT III for different L_S , $L_{S,2}$, and L_V : (a) $L_S = 3D$; (b) $L_S = 7D$.

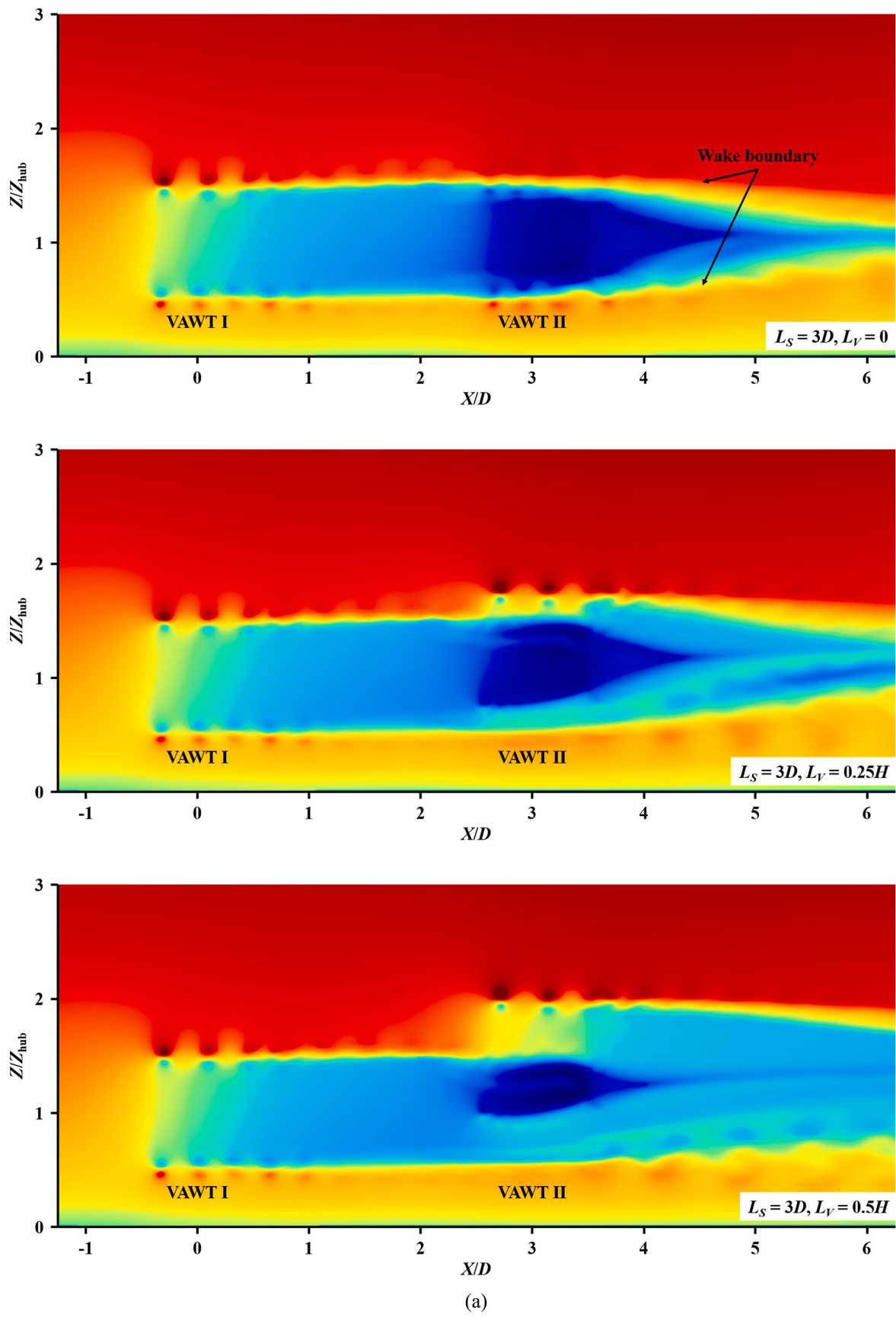


Fig. 11. Instantaneous velocity distribution around the turbine array in the vertical plane ($Y = 0$) for different L_S and L_V : (a) $L_S = 3D$; (b) $L_S = 7D$.

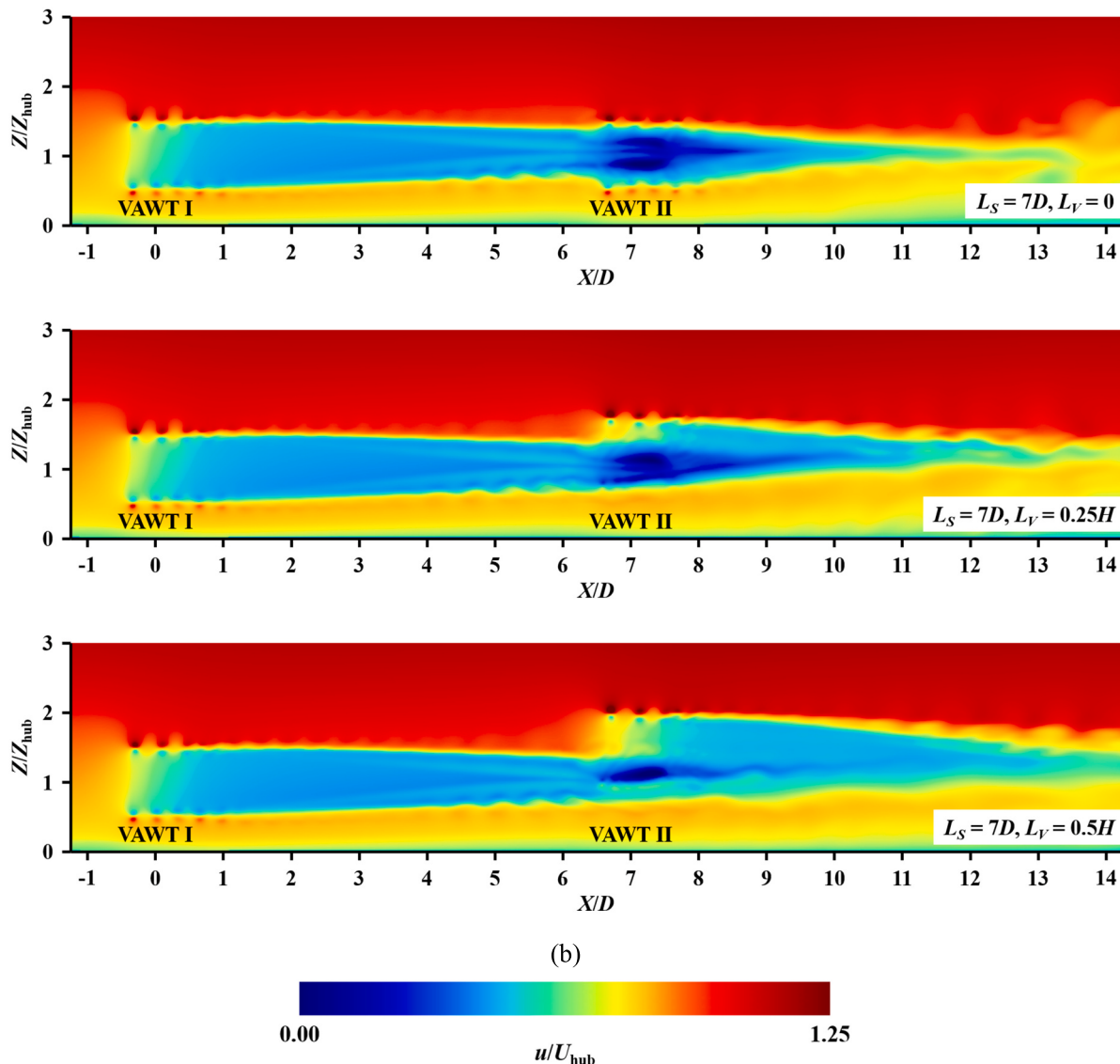


Fig. 11. (continued).

Fig. 9), supporting the results shown in **Fig. 10**. Therefore, with relatively large turbine spacing, the vertically staggered arrangement may negatively affect the aerodynamics of VAWT III. Nevertheless, the vertically staggered arrangement is anticipated to mitigate wake interference in offshore wind farms consisting of VAWTs. Although the power output of VAWT III may decrease, the strong wake interference acting on it will promote the wake recovery, benefiting the VAWT further downstream. This means that when the turbine array comprises an even number of VAWTs, the vertically staggered arrangement can effectively increase the total power output.

Fig. 12 shows the instantaneous vortical structures around the turbine array for different L_S and L_V . It can be observed that for $L_S = 3D$, when the two VAWTs are aligned, spanwise and tip vortices periodically shed from VAWT I and move downstream, fully mixing with the wake structures of VAWT II. The strong wake interference increases the turbulence level in the wake of VAWT II, resulting in high instability and promoting the breakup of vortices, which contributes to fast wake recovery. As the wake develops, large-scale vortices emerge and strong vortex interactions are observed. This phenomenon was also observed in visualization experiments by Araya et al. [71]. They noted that these large structures were the result of the developing shear layer instability

in the turbine wake and appeared to dominate the flow dynamics in the far wake region. The strong instability leads to the collapse of shear layers, which promotes turbulent production and vortex reconstitution [17,19]. In the case of vertically staggered arrangement, as VAWT II avoids partial wake interference from VAWT I, the breakup of vortices is delayed and the vortex interactions are weakened, especially for $L_V = 0.5H$. In this scenario, the wake structures of the turbine array develop stably downstream. For $L_S = 7D$, the wake interference acting on VAWT II is weaker than that for $L_S = 3D$, making the wake structures of VAWT II more stable. Also, the added turbulence energizes the wake of VAWT II and mitigates the early breakup of vortices. In addition, the vertically staggered arrangement makes the wake of VAWT II less affected by the upstream interference, weakening the vortex interactions and contributing to the relatively slow wake recovery shown in **Fig. 11**.

In addition, Supplementary material S.5 provides an investigation of the impact of wind direction on wake interference between two vertically staggered VAWTs.

5. Wake interference between combined staggered turbines

This section investigates the wake interference between two

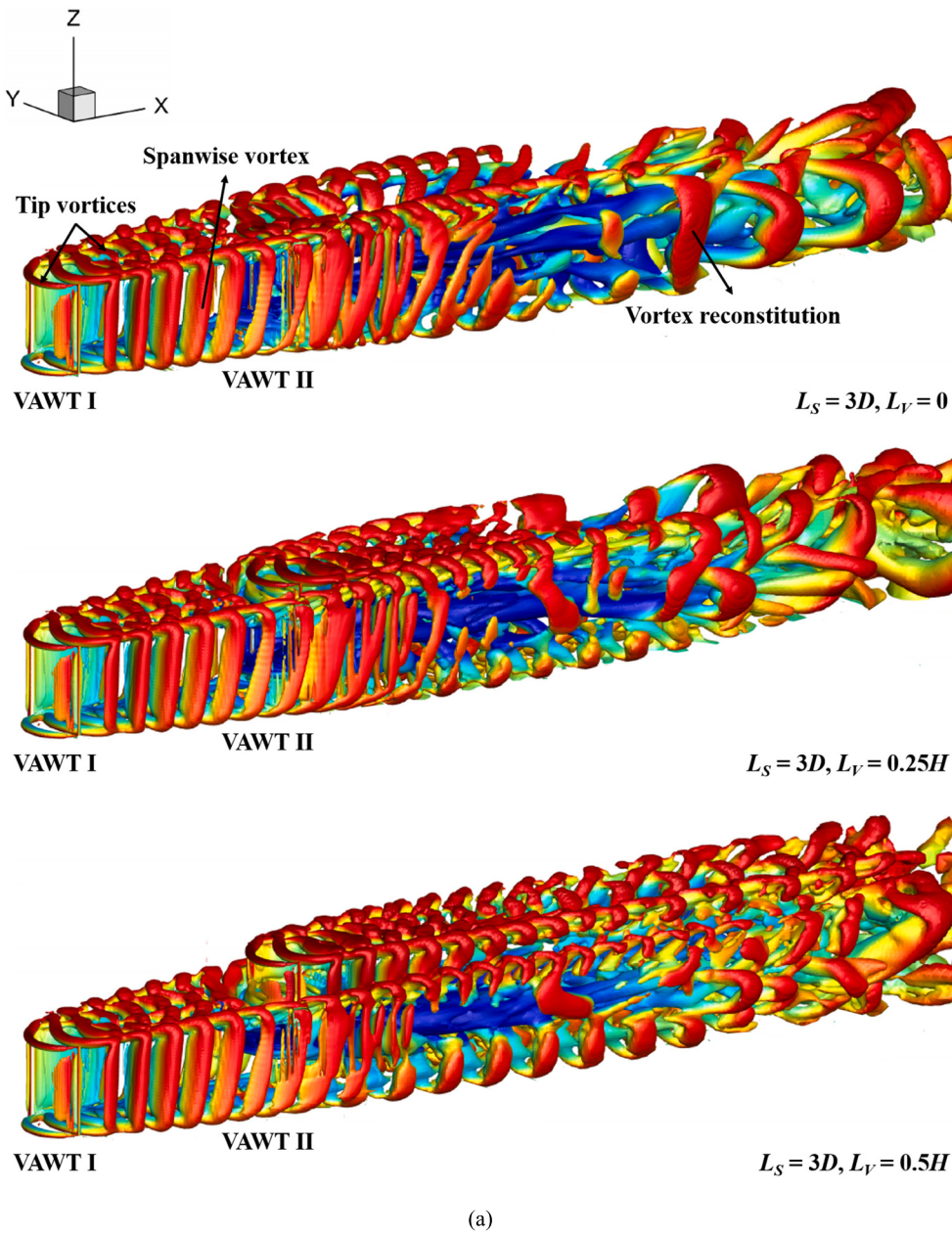


Fig. 12. Instantaneous vortical structures around the turbine array for different L_s and L_v : (a) $L_s = 3D$; (b) $L_s = 7D$.

combined staggered VAWTs. The objectives are twofold: firstly, to compare the effectiveness of horizontally and vertically staggered arrangements in mitigating wake interference within the turbine array, and secondly, to identify the relatively optimal layout of the turbine array. Three separation distances of $L_s = 3D$, $5D$, and $7D$ are considered. Three vertically staggered distances of $L_v = \pm 0.25H$ and $0.5H$ and three horizontally staggered distances of $L_h = \pm 0.25D$ and $-0.5D$ are selected for VAWT II. A negative L_h of $-0.5D$ is selected due to the typically smaller velocity deficit on the leeward side ($Y < 0$) of VAWT I compared to the windward side ($Y > 0$), which is a result of the Magnus effect [72]. Both VAWTs operate at a rotational speed of 12 rpm.

5.1. Taguchi method

The Taguchi method is a statistical technique developed to optimize the quality of a product or process while minimizing cost and reducing variation [73]. It can utilize orthogonal experimental designs to

evaluate the impact of factors with fewer runs. For CFD-based parametric studies, the Taguchi method can reduce the number of CFD cases and preserve the characteristics of the parameter space [74]. This method has been employed in many VAWT studies [75–78], demonstrating its reliability in parametric analysis and optimization. Here, the Taguchi method is employed to design numerical experiments (i.e., CFD simulations), evaluate the impact of different spatial factors (i.e., separation and staggered distances), and identify the optimal configuration of these factors (i.e., relatively optimal layout of the turbine array).

Fig. 13 shows a flowchart of the Taguchi method. The details of the steps are as follows:

- 1) Define the objective function. The Taguchi method uses the signal-to-noise (S/N) ratio to analyze the quality characteristics of product or process parameters [75]. Based on previous studies [78,79], the larger-the-better type S/N ratio is selected as the objective function, expressed as:

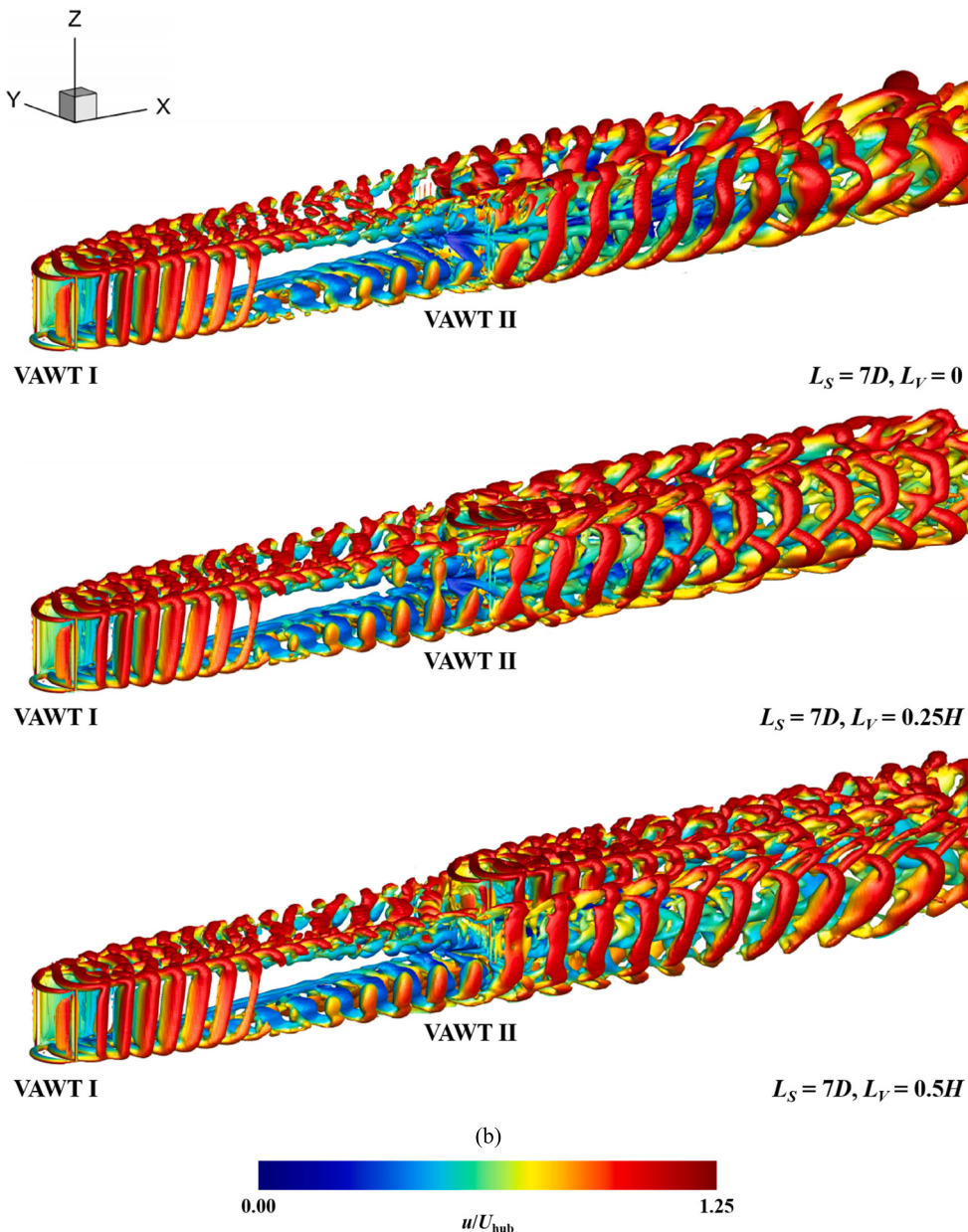


Fig. 12. (continued).

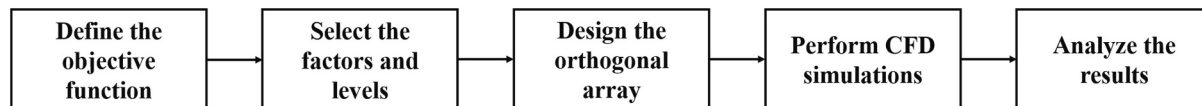


Fig. 13. Flowchart of the Taguchi method.

$$S/N = -10 \log \left(\frac{\sum_{i=1}^n \frac{1}{y_i^2}}{n} \right) \quad (1)$$

where y_i denotes the sample value (i.e., normalized power output of the turbine array $P_{\text{nor}}^{\text{Overall}}$) and n denotes the sample number, which is equal to 1 in this study. Larger-the-better means that the larger the ratio value, the better the product quality (i.e., higher $P_{\text{nor}}^{\text{Overall}}$).

Table 4
Factors and levels.

Factor	Level 1	Level 2	Level 3
A, separation distance L_S	3D	5D	7D
B, vertically staggered distance L_V	-0.25H	0.25H	0.5H
C, horizontally staggered distance L_H	-0.5D	-0.25D	0.25D

Table 5
Orthogonal array.

Numerical experiment	A (L_S)	B (L_V)	C (L_H)
1	1 (3D)	1 (-0.25H)	1 (-0.5D)
2	1 (3D)	2 (0.25H)	2 (-0.25D)
3	1 (3D)	3 (0.5H)	3 (0.25D)
4	2 (5D)	1 (-0.25H)	2 (-0.25D)
5	2 (5D)	2 (0.25H)	3 (0.25D)
6	2 (5D)	3 (0.5H)	1 (-0.5D)
7	3 (7D)	1 (-0.25H)	3 (0.25D)
8	3 (7D)	2 (0.25H)	1 (-0.5D)
9	3 (7D)	3 (0.5H)	2 (-0.25D)

Table 6
Results of the orthogonal array.

Numerical experiment	A (L_S)	B (L_V)	C (L_H)	$P_{\text{nor}}^{\text{Overall}}$	S/N ratio
1	1 (3D)	1 (-0.25H)	1 (-0.5D)	0.7022	-3.0708
2	1 (3D)	2 (0.25H)	2 (-0.25D)	0.6519	-3.7164
3	1 (3D)	3 (0.5H)	3 (0.25D)	0.8084	-1.8475
4	2 (5D)	1 (-0.25H)	2 (-0.25D)	0.64	-3.8764
5	2 (5D)	2 (0.25H)	3 (0.25D)	0.6129	-4.2522
6	2 (5D)	3 (0.5H)	1 (-0.5D)	0.905	-0.867
7	3 (7D)	1 (-0.25H)	3 (0.25D)	0.59	-4.583
8	3 (7D)	2 (0.25H)	1 (-0.5D)	0.7126	-2.9431
9	3 (7D)	3 (0.5H)	2 (-0.25D)	0.9383	-0.5532

Table 7
Results of the mean S/N ratio and the degree of impact.

Factor/ level	S/N ratio			Mean S/N ratio	Degree of impact
	j = 1	j = 2	j = 3		
A/1	-3.0708	-3.7164	-1.8475	-2.8782	
A/2	-3.8764	-4.2522	-0.867	-2.9985	0.3054
A/3	-4.583	-2.9431	-0.5532	-2.6931	
B/1	-3.0708	-3.8764	-4.583	-3.8434	
B/2	-3.7164	-4.2522	-2.9431	-3.6372	2.7542
B/3	-1.8475	-0.867	-0.5532	-1.0892	
C/1	-3.0708	-0.867	-2.9431	-2.2936	
C/2	-3.7164	-3.8764	-0.5532	-2.7153	1.2673
C/3	-1.8475	-4.2522	-0.4583	-3.5609	

- 2) Select the factors and levels, design the orthogonal array, and perform CFD simulations. Table 4 lists the factors and levels considered in this study. Based on the standard four-factor three-level orthogonal array L9 (3⁴), a three-factor three-level orthogonal array is obtained by dropping the fourth factor, as listed in Table 5. This results in a total of nine CFD cases.
- 3) Analyze the results. Based on the S/N ratio analysis, this step evaluates the impact of different factors and identifies their optimal configuration. The optimal configuration is identified by comparing the mean S/N ratio of factors at different levels. The larger the mean S/N ratio, the better the factor level. The combination of the best levels of each factor is the optimal configuration. For example, the mean S/N ratio of factor A at level i is calculated as:

$$M_{A_i} = \frac{1}{n_{A_i}} \sum_{j=1}^{n_{A_i}} [(S/N)_{A_i}]_j \quad (2)$$

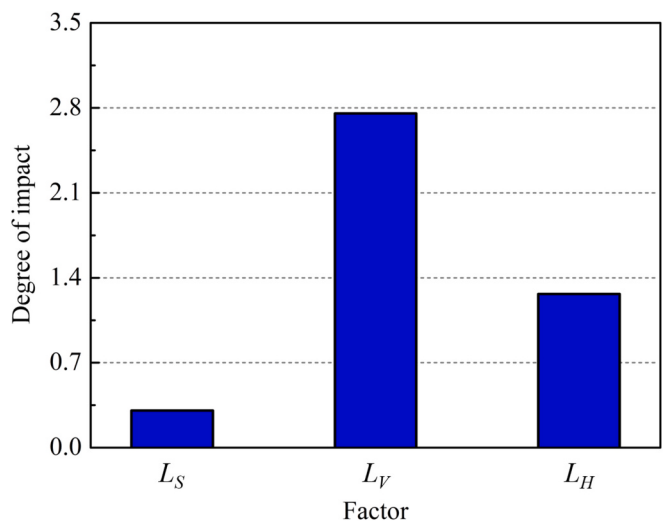


Fig. 14. Comparison of degree of impact of different factors.

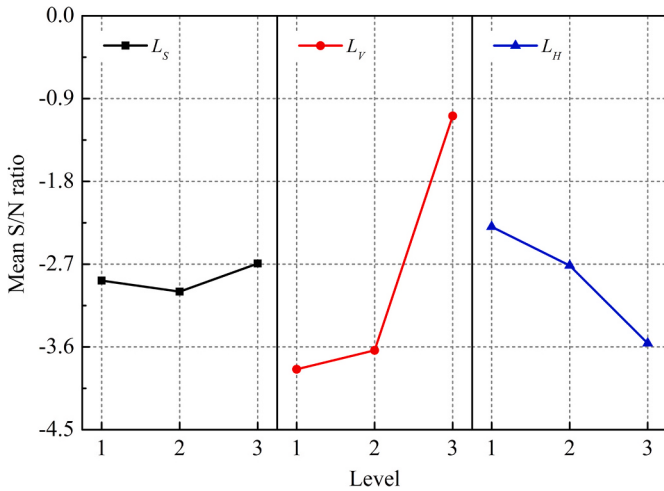


Fig. 15. Mean S/N ratio of factors at different levels.

where n_{A_i} denotes the number of occurrences of factor A at level i, which is equal to 3 in this study, and j denotes the jth occurrence of factor A at level i. The impact of factors, on the other hand, is evaluated by the difference between the maximum and minimum mean S/N ratios. The larger the difference, the higher the degree of impact of the factor. For example, the degree of impact of factor A is calculated as:

$$D_A = \max(M_{A_1}, M_{A_2}, \dots, M_{A_i}) - \min(M_{A_1}, M_{A_2}, \dots, M_{A_i}) \quad (3)$$

5.2. Signal-to-noise ratio analysis

Table 6 lists the results of the orthogonal array. Table 7 lists the results of the mean S/N ratio and the degree of impact. To visualize the results, Fig. 14 compares the degree of impact of different factors. It can be observed that the degree of impact ranks as $L_V > L_H > L_S$. On the one hand, the staggered distance has a greater impact on wake interference than the separation distance, demonstrating the significance of staggered arrangement in optimizing the layout of offshore wind farms. On the other hand, the vertically staggered arrangement allows the turbine array to achieve higher power output than the horizontally staggered arrangement for the same staggered distance, indicating its potential in mitigating wake interference between VAWTs.

Fig. 15 shows the mean S/N ratio of factors at different levels. It can

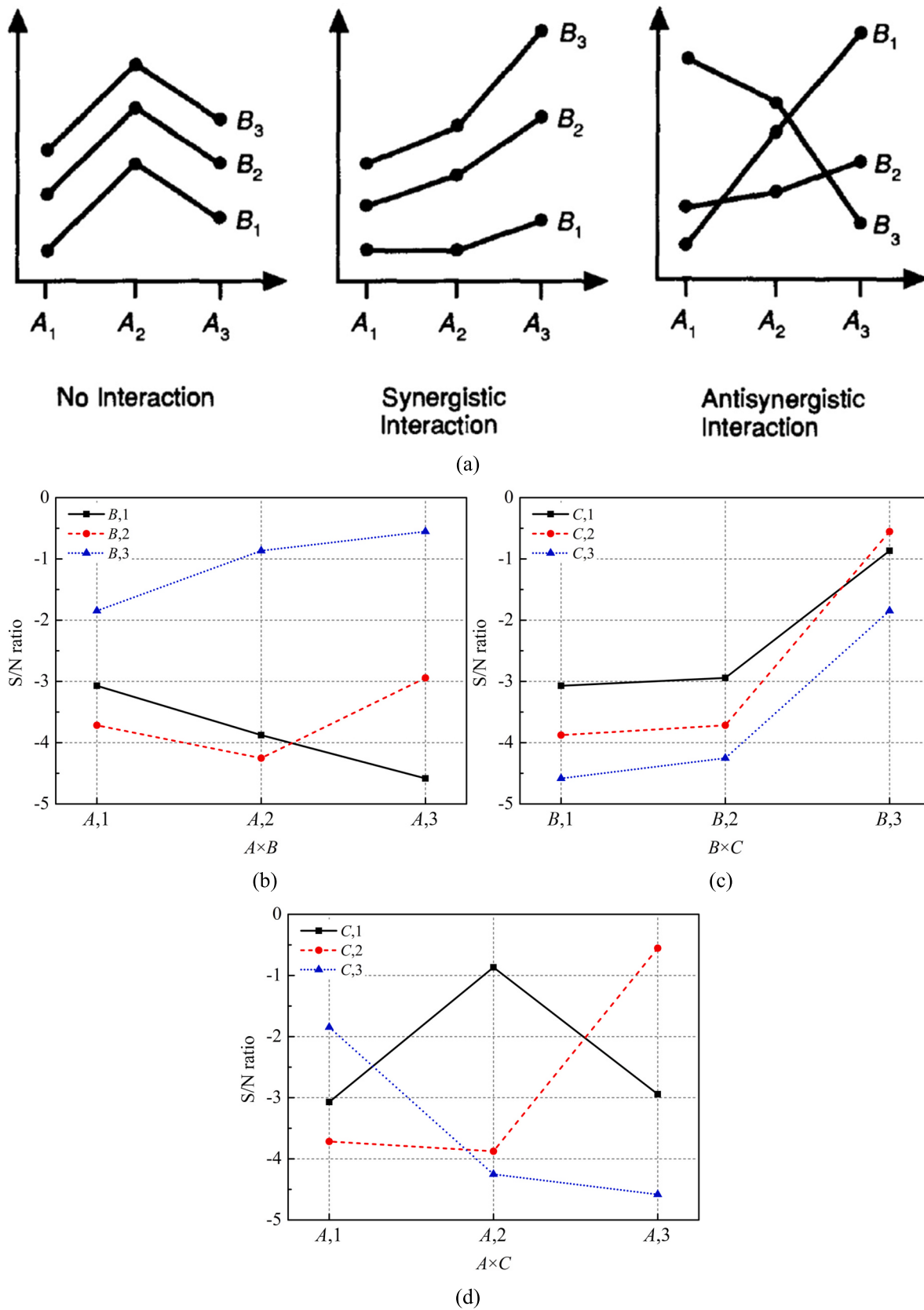


Fig. 16. Interaction profiles of any two factors: (a) example [82]; (b) A and B; (c) B and C; (d) A and C.

Table 8
Results of the predicted S/N ratio.

Case	A (L_S)	B (L_V)	C (L_H)	Predicted S/N ratio
1	1 (3D)	1 (-0.25H)	1 (-0.5D)	-3.0538
2	1 (3D)	1 (-0.25H)	2 (-0.25D)	-4.0833
3	1 (3D)	1 (-0.25H)	3 (0.25D)	-2.0754
4	1 (3D)	2 (0.25H)	1 (-0.5D)	-3.7778
5	1 (3D)	2 (0.25H)	2 (-0.25D)	-4.775
6	1 (3D)	2 (0.25H)	3 (0.25D)	-2.5964
7	1 (3D)	3 (0.5H)	1 (-0.5D)	-2.3808
8	1 (3D)	3 (0.5H)	2 (-0.25D)	-2.2909
9	1 (3D)	3 (0.5H)	3 (0.25D)	-8.7076
10	2 (5D)	1 (-0.25H)	1 (-0.5D)	-1.5353
11	2 (5D)	1 (-0.25H)	2 (-0.25D)	-4.9286
12	2 (5D)	1 (-0.25H)	3 (0.25D)	-5.1654
13	2 (5D)	2 (0.25H)	1 (-0.5D)	-1.9895
14	2 (5D)	2 (0.25H)	2 (-0.25D)	-5.3505
15	2 (5D)	2 (0.25H)	3 (0.25D)	-5.4166
16	2 (5D)	3 (0.5H)	1 (-0.5D)	0.9238
17	2 (5D)	3 (0.5H)	2 (-0.25D)	-1.3501
18	2 (5D)	3 (0.5H)	3 (0.25D)	-2.1747
19	3 (7D)	1 (-0.25H)	1 (-0.5D)	-4.6234
20	3 (7D)	1 (-0.25H)	2 (-0.25D)	-2.6174
21	3 (7D)	1 (-0.25H)	3 (0.25D)	-6.5082
22	3 (7D)	2 (0.25H)	1 (-0.5D)	-3.062
23	3 (7D)	2 (0.25H)	2 (-0.25D)	-1.0237
24	3 (7D)	2 (0.25H)	3 (0.25D)	-4.7437
25	3 (7D)	3 (0.5H)	1 (-0.5D)	-1.144
26	3 (7D)	3 (0.5H)	2 (-0.25D)	1.9814
27	3 (7D)	3 (0.5H)	3 (0.25D)	-2.4971

be observed that the mean S/N ratio first increases then decreases with the increase of L_S . Superior power performance can be expected for $L_S = 7D$, as the wake of the upstream turbine gradually recovers with the increase of L_S . However, the power output of the turbine array for $L_S = 5D$ is unexpectedly lower than that for $L_S = 3D$. The explanation for this surprising result will be provided in the subsequent section. For L_V , the trend of $0.5H > 0.25H > -0.25H$ aligns with the results in Section 4, and the performance improvement of the turbine array is significant when L_V increases from $0.25H$ to $0.5H$. For L_H , the trend of $-0.5D > -0.25D > 0.25D$ is also expected. On the one hand, a larger absolute value of L_H allows the downstream turbine to avoid more wake interference from the upstream one. On the other hand, due to the Magnus effect, the wake velocity on the leeward side is generally higher than that on the windward side, therefore the power output of VAWT II will be higher when L_H is negative. As such, it can be concluded that the optimal configuration of factors is $L_S = 7D$, $L_V = 0.5H$, and $L_H = -0.5D$. It should be noted that the optimization of the Taguchi method is constrained by the factor levels [80]. While global optimization methods such as genetic algorithm (GA) and particle swarm optimization (PSO) can provide more accurate identification, they are hampered by high computational cost, slow convergence, or swarm stagnation [81]. In addition, these methods are inconsistent with the research objective of this study to evaluate the impact of factors. Considering these issues, GA and PSO are not selected for this study.

5.3. Factor interaction and modified additive model

As described above, the optimal configuration of the factors is $L_S = 7D$, $L_V = 0.5H$, and $L_H = -0.5D$. However, the numerical results show that the $P_{\text{nor}}^{\text{Overall}}$ for the optimal case is 0.9064, which is lower than that for $L_S = 7D$, $L_V = 0.5H$, and $L_H = -0.25D$. According to previous study [76], the reason for this phenomenon may be the interactions between the considered factors, leading to an inaccurate identification of the optimal configuration. To verify this assumption, Fig. 16 shows the interaction profiles of any two factors. As shown in Fig. 16(a), if there is no interaction between the two factors, the profile will exhibit parallelism, while non-parallelism suggests that the two factors are interacting with each other. Also, if there is an antisynergistic (strong)

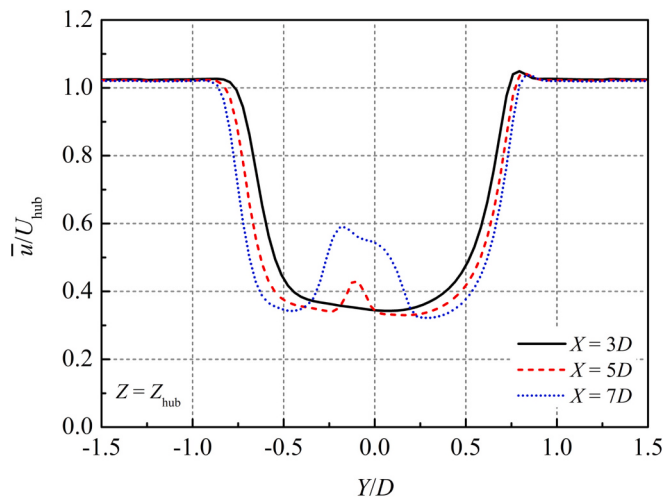


Fig. 17. Normalized mean wake profiles of VAWT I in the horizontal plane ($Z = Z_{\text{hub}}$) for different downstream distances.

interaction, the interactions between the factors must be taken into account in the Taguchi method. It can be observed that the L_S - L_V and L_V - L_H pairs show a synergistic (weak) interaction. However, there is an antisynergistic interaction between L_S and L_H , indicating that the impact of L_H on the power performance of the turbine array exhibits different characteristics for different L_S . This strong interaction leads to the inaccurate identification of the optimal configuration.

To address the above issue, a modified additive model is employed in this study to include the interaction effect of factors. Its main idea is to consider the contribution of the interaction of any two factors in the S/N ratio analysis and to add the contribution term to the equation for predicting the S/N ratio [76,77]. For example, the contributing term of the interaction between factor A at level i and factor B at level j is calculated as [76]:

$$C_{A_i, B_j} = (M_{A_i, B_j} - M) - (M_{A_i} - M) - (M_{B_j} - M) \quad (4)$$

where M_{A_i, B_j} denotes the mean S/N ratio of the cases including both A_i and B_j . M denotes the mean S/N ratio of all cases in the orthogonal array. Then, the predicted S/N ratio of the possible configurations of factors is calculated as [76]:

$$E_{A_i, B_j, C_k} = M + M_{a_i} + M_{b_j} + M_{c_k} + C_{A_i, B_j} + C_{B_j, C_k} + C_{A_i, C_k} \quad (5)$$

where $M_{a_i} = M_{A_i} - M$, $M_{b_j} = M_{B_j} - M$, and $M_{c_k} = M_{C_k} - M$. The maximum E_{A_i, B_j, C_k} is expected to correspond to the optimal configuration of factors.

Table 8 lists the results of the predicted S/N ratio. From this, it can be observed that case 26 has the maximum predicted S/N ratio, corresponding to a configuration of $L_S = 7D$, $L_V = 0.5H$, and $L_H = -0.25D$. Also, the results of the orthogonal array show that this configuration has the highest $P_{\text{nor}}^{\text{Overall}}$ of 0.9383, which is 46.27% higher than the aligned case of $L_S = 7D$. Hence, the modified additive model is proven to accurately predict the optimal configuration of the considered factors.

5.4. Mechanism exploration

In this section, the aerodynamic mechanisms behind two previously mentioned phenomena are explored. Firstly, the reason why the power performance of the turbine array for $L_S = 5D$ is inferior to that for $L_S = 3D$. Secondly, the reason why the impact of L_H exhibits different characteristics for different L_S , especially why $P_{\text{nor}}^{\text{Overall}}$ for $L_S = 7D$, $L_V = 0.5H$, and $L_H = -0.5D$ is lower than that for $L_S = 7D$, $L_V = 0.5H$, and $L_H = -0.25D$.

Fig. 17 shows the normalized mean wake profiles of VAWT I in the

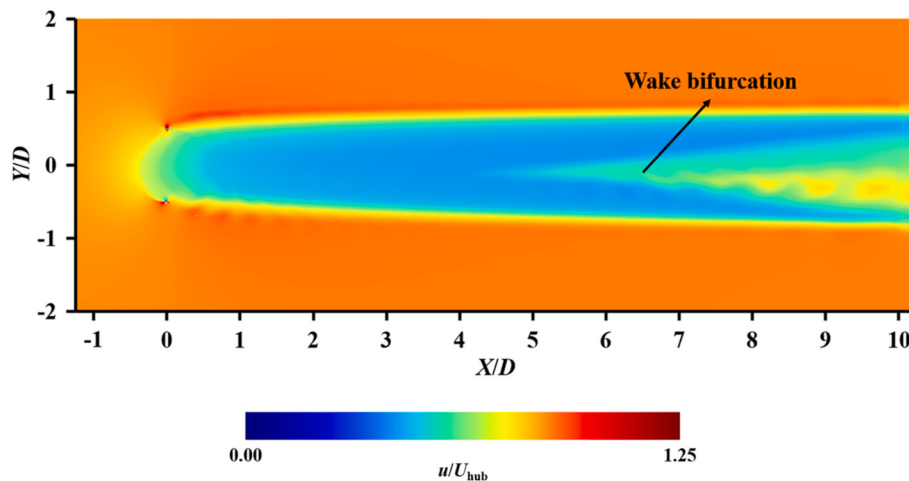


Fig. 18. Instantaneous velocity distribution around the stand-alone VAWT in the horizontal plane ($Z = Z_{\text{hub}}$).

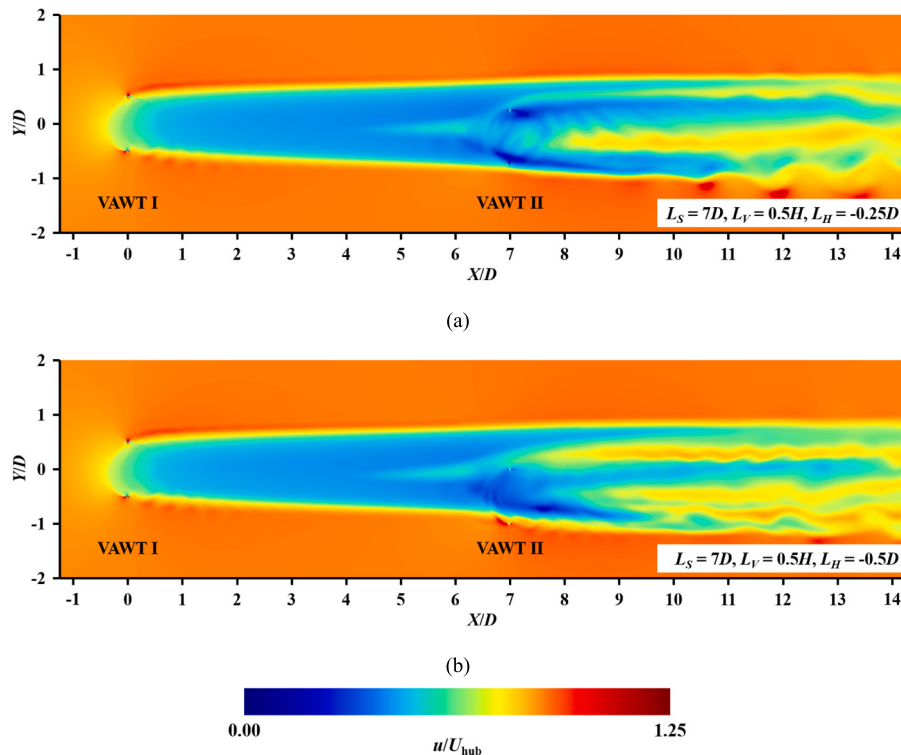


Fig. 19. Instantaneous velocity distribution around the turbine array in the horizontal plane ($Z = Z_{\text{hub}}$) for different L_H : (a) $L_H = -0.25D$; (b) $L_H = -0.5D$.

horizontal plane ($Z = Z_{\text{hub}}$) for different downstream distances. The wake boundary of VAWT I is observed to expand with increasing downstream distance, where the velocity deficit in the ranges of $Y = (-0.75D, 0.5D)$ and $(0.25D, 0.75D)$ increases. Also, the wake velocity in the range of $Y = (-0.25D, 0.25D)$ for $X = 7D$ is significantly higher than that for $X = 3D$ and $5D$, indicating the recovery of turbine wake. This asymmetric W-shaped velocity profile was also reported in the wind tunnel tests conducted by Peng et al. [83]. For $X = 5D$, although the velocity deficit in the range of $Y = (-0.25D, 0)$ is slightly smaller than that for $X = 3D$, the lower wake velocity in the remaining range of the wake region negatively affects the aerodynamics of the downstream turbine, lowering the mean S/N ratio.

Fig. 18 shows the instantaneous velocity distribution around the stand-alone VAWT in the horizontal plane ($Z = Z_{\text{hub}}$). It can be observed

that when $X > 5D$, a clear bifurcation occurs in the turbine wake, forming a relatively high-velocity region around the centerline ($Y = 0$). This corresponds to the significant increase of the wake velocity in the range of $Y = (-0.25D, 0.25D)$ for $X = 7D$ shown in Fig. 16. This wake bifurcation is a result of the Magnus effect and wake instability, as reported in previous studies [22,83]. This physical phenomenon changes the law of the impact of L_H on the power performance of the turbine array. As can be observed in Fig. 19, when $L_H = -0.5D$, VAWT II moves away from the centerline and towards the low-velocity region on the leeward side. Compared to the case of $L_H = -0.25D$, although VAWT II avoids more wake interference on the windward side when $L_H = -0.5D$, the benefit of the high-velocity region is diminished, leading to a decrease in $P_{\text{nor}}^{\text{II}}$ and $P_{\text{nor}}^{\text{Overall}}$. This observation is confirmed by the comparison of instantaneous $Q_{\text{nor}}^{\text{II}}$ shown in Fig. 20, where the $Q_{\text{nor}}^{\text{II}}$ decreases

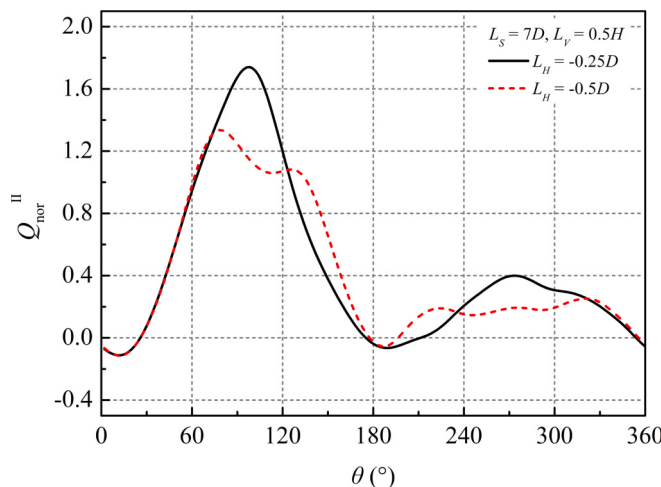


Fig. 20. Comparison of instantaneous Q_{nor}^H (blade) for different L_H .

significantly in the regions of $60^\circ < \theta \leq 120^\circ$ and $240^\circ \leq \theta \leq 300^\circ$ for $L_H = -0.5D$. Therefore, when L_S is relatively small, a larger L_H allows the downstream turbine to achieve a higher power output. Conversely, when L_S is relatively large, a smaller L_H is more conducive to the performance improvement of the turbine array.

6. Conclusions

The impact of vertically staggered arrangement on wake interference remains ambiguous. This study, therefore, evaluates the effectiveness of such arrangement in mitigating wake interference between offshore VAWTs. Using high-fidelity CFD simulations, the wake interference between two vertically staggered MW-class VAWTs is investigated. Also, to clarify the difference between horizontally and vertically staggered arrangements, the Taguchi method is employed to analyze the power output of two combined staggered VAWTs. This approach aids in identifying the relatively optimal layout of the turbine array. The main findings include:

- The vertically staggered arrangement allows the downstream turbine to avoid partial wake interference from the upstream one, leading to a significant performance improvement, e.g., the power output increases by 75.96% when $L_S = 7D$ and $L_V = 0.25H$. For basic two-turbine arrays with relatively large turbine spacing (i.e., $L_S \geq 3D$), VAWTs are inferior to HAWTs due to the slow wake recovery of existing conceptual MW-class VAWTs.
- For a relatively small L_S (e.g., $3D$), a negative L_V is suggested, as it can reduce the tower cost while preserving the performance improvement; for a relatively large L_S (e.g., $7D$), a positive L_V is suggested, as it can bring considerable performance improvement and compensate for the negative impact of increased hub height.
- The staggered distance has a greater impact on wake interference than the separation distance. For the same staggered distance, the vertically staggered arrangement allows the turbine array to achieve higher power output than the horizontally staggered arrangement.
- The wake bifurcation makes the impact of L_H exhibit different characteristics for different L_S . For a relatively small L_S (e.g., $3D$ and $5D$), a larger L_H allows the downstream turbine to achieve a higher power output, while for a relatively large L_S (e.g., $7D$), a smaller L_H is more conducive to the performance improvement of the turbine array.
- The modified additive model can improve the accuracy of the Taguchi method in identifying the optimal configuration when there are strong interactions between the factors. Given the factors and levels considered, the relatively optimal layout of the turbine array is

$L_S = 7D$, $L_V = 0.5H$, and $L_H = -0.25D$. The power output of the turbine array is increased by 46.27% compared to the aligned case of $L_S = 7D$.

In summary, this study provides a comprehensive evaluation of the feasibility of staggered arrangement in increasing the power output of VAWT arrays. The findings may contribute to the layout design of offshore wind farms.

CRediT authorship contribution statement

Limin Kuang: Conceptualization, Formal analysis, Methodology, Software, Validation, Writing – original draft. **Hiroshi Katsuchi:** Supervision, Writing – review & editing. **Dai Zhou:** Funding acquisition, Resources, Supervision, Writing – review & editing. **Yaoran Chen:** Writing – review & editing. **Zhaolong Han:** Funding acquisition, Resources, Supervision. **Kai Zhang:** Supervision, Writing – review & editing. **Jiaqi Wang:** Writing – review & editing. **Yan Bao:** Supervision. **Yong Cao:** Supervision. **Yijie Liu:** Writing – review & editing.

Declaration of Competing Interest

The authors declare that they have no known competing financial interests or personal relationships that could have appeared to influence the work reported in this paper.

Data availability

Data will be made available on request.

Acknowledgments

The financial supports from the Innovation Program of Shanghai Municipal Education Commission (No. 2019-01-07-00-02-E00066), National Natural Science Foundation of China (Nos. 52122110 and 42076210), Shuguang Program of Shanghai Education Development Foundation and Shanghai Municipal Education Commission (No. 19SG10), Oceanic Interdisciplinary Program of Shanghai Jiao Tong University (No. SL2020PT201), and China Scholarship Council (No. 202206230089) are gratefully acknowledged.

Appendix A. Supplementary data

Supplementary data to this article can be found online at <https://doi.org/10.1016/j.apenergy.2023.121850>.

References

- [1] Breton SP, Moe G. Status, plans and technologies for offshore wind turbines in Europe and North America. *Renew Energy* 2009;34(3):646–54.
- [2] Hand B, Kelly G, Cashman A. Aerodynamic design and performance parameters of a lift-type vertical axis wind turbine: a comprehensive review. *Renew Sustain Energy Rev* 2021;139:110699.
- [3] Zhang D, Zhang X, He J, Chai Q. Offshore wind energy development in China: current status and future perspective. *Renew Sustain Energy Rev* 2011;15(9): 4673–84.
- [4] Xia J, Zou G. Operation and maintenance optimization of offshore wind farms based on digital twin: a review. *Ocean Eng* 2023;268:11322.
- [5] Lei H, Zhou D, Bao Y, Li Y, Han Z. Three-dimensional improved delayed detached Eddy simulation of a two-bladed vertical axis wind turbine. *Energy Conv Manag* 2017;133:235–48.
- [6] Ghaseemian M, Najafian Ashrafi Z, Sedaghat A. A review on computational fluid dynamic simulation techniques for Darrieus vertical axis wind turbines. *Energy Conv Manag* 2017;149:87–100.
- [7] Elkhouri M, Kiwata T, Aoun E. Experimental and numerical investigation of a three-dimensional vertical-axis wind turbine with variable-pitch. *J Wind Eng Ind Aerodyn* 2015;139:111–23.
- [8] Wang Z, Zhuang M. Leading-edge serrations for performance improvement on a vertical-axis wind turbine at low tip-speed-ratios. *Appl Energy* 2017;208:1184–97.
- [9] Rezaeiha A, Montazeri H, Blocken B. Active flow control for power enhancement of vertical axis wind turbines: leading-edge slot suction. *Energy* 2019;189:116131.

- [10] Rezaieha A, Montazeri H, Blocken B. Characterization of aerodynamic performance of vertical axis wind turbines: impact of operational parameters. *Energy Conv Manag* 2018;169:45–77.
- [11] Li G, Xu W, Li Y, Wang F. Univariate analysis of scaling effects on the aerodynamics of vertical axis wind turbines based on high-resolution numerical simulations: the Reynolds number effects. *J Wind Eng Ind Aerodyn* 2022;223:104938.
- [12] Ishihara T, Qian G. A new Gaussian-based analytical wake model for wind turbines considering ambient turbulence intensities and thrust coefficient effects. *J Wind Eng Ind Aerodyn* 2018;177:275–92.
- [13] Chen G, Li X, Liang X. IDDES simulation of the performance and wake dynamics of the wind turbines under different turbulent inflow conditions. *Energy* 2022;238:121772.
- [14] Barthelmie RJ, Hansen K, Frandsen ST, Rathmann O, Schepers JG, Schlez W, et al. Modelling and measuring flow and wind turbine wakes in large wind farms offshore. *Wind Energy* 2009;12(5):431–44.
- [15] Nilsson K, Ivanell S, Hansen KS, Mikkelsen R, Sørensen JN, Breton SP, et al. Large-eddy simulations of the Lillgrund wind farm. *Wind Energy* 2015;18(3):449–67.
- [16] Hohman TC, Martinelli L, Smits AJ. The effects of inflow conditions on vertical axis wind turbine wake structure and performance. *J Wind Eng Ind Aerodyn* 2018;183:1–18.
- [17] Posa A. Influence of tip speed ratio on wake features of a vertical Axis wind turbine. *J Wind Eng Ind Aerodyn* 2020;197:104076.
- [18] Lei H, Su J, Bao Y, Chen Y, Han Z, Zhou D. Investigation of wake characteristics for the offshore floating vertical axis wind turbines in pitch and surge motions of platforms. *Energy* 2019;166:471–89.
- [19] Posa A. Dependence of the wake recovery downstream of a vertical Axis wind turbine on its dynamic solidity. *J Wind Eng Ind Aerodyn* 2020;202:104212.
- [20] Shamsoddin S, Porté-Agel F. Effect of aspect ratio on vertical-axis wind turbine wakes. *J Fluid Mech* 2020;889:R1.
- [21] Zuo W, Wang X, Kang S. Numerical simulations on the wake effect of H-type vertical axis wind turbines. *Energy* 2016;106:691–700.
- [22] Kuang L, Lei H, Zhou D, Han Z, Bao Y, Zhao Y. Numerical investigation of effects of turbulence intensity on aerodynamic performance for straight-bladed vertical-axis wind turbines. *J Energy Eng-ASCE* 2021;147(1):04020087.
- [23] Kuang L, Lu Q, Huang X, Song L, Chen Y, Su J, et al. Characterization of wake interference between two tandem offshore floating vertical-axis wind turbines: effect of platform pitch motion. *Energy Conv Manag* 2022;265:115769.
- [24] Kinzel M, Mulligan Q, Dabiri JO. Energy exchange in an array of vertical-axis wind turbines. *J Turbul* 2012;13:1–13.
- [25] Ahmadi-Baloutaki M, Carriveau R, Ting DS. A wind tunnel study on the aerodynamic interaction of vertical axis wind turbines in array configurations. *Renew Energy* 2016;96:904–13.
- [26] Su H, Meng H, Qu T, Lei L. Wind tunnel experiment on the influence of array configuration on the power performance of vertical axis wind turbines. *Energy Conv Manag* 2021;241:114299.
- [27] Dabiri JO. Potential order-of-magnitude enhancement of wind farm power density via counter-rotating vertical-axis wind turbine arrays. *J Renew Sustain Energy* 2011;3(4):043104.
- [28] Zanforlin S, Nishino T. Fluid dynamic mechanisms of enhanced power generation by closely spaced vertical axis wind turbines. *Renew Energy* 2016;99:1213–26.
- [29] Alexander AS, Santhanakrishnan A. Mechanisms of power augmentation in two side-by-side vertical axis wind turbines. *Renew Energy* 2020;148:600–10.
- [30] Sahebzadeh S, Rezaieha A, Montazeri H. Vertical-axis wind-turbine farm design: impact of rotor setting and relative arrangement on aerodynamic performance of double rotor arrays. *Energy Rep* 2022;8:5793–819.
- [31] Peng H, Han Z, Liu H, Lin K, Lam H. Assessment and optimization of the power performance of twin vertical axis wind turbines via numerical simulations. *Renew Energy* 2020;147:43–54.
- [32] Chen Y, Kuang L, Su J, Zhou D, Cao Y, Chen H, et al. Investigation of pitch angles on the aerodynamics of twin-VAWT under staggered arrangement. *Ocean Eng* 2022;254:111385.
- [33] Yang X, Kang S, Sotropoulos F. Computational study and modeling of turbine spacing effects in infinite aligned wind farms. *Phys Fluids* 2012;24(11):115107.
- [34] Hamilton N, Melius M, Cai RB. Wind turbine boundary layer arrays for Cartesian and staggered configurations-Part I, flow field and power measurements. *Wind Energy* 2015;18(2):277–95.
- [35] Tian W, Ozbay A, Hu H. An experimental investigation on the wake interferences among wind turbines sited in aligned and staggered wind farms. *Wind Energy* 2018;21(2):100–14.
- [36] Dot B, Guala M, Zeng P, Lei L. Experimental investigation of the power performance of a minimal wind turbine array in an atmospheric boundary layer wind tunnel. *Energy Conv Manag* 2019;196:906–19.
- [37] Vasel-Be-Hagh A, Archer CL. Wind farm hub height optimization. *Appl Energy* 2017;195:905–21.
- [38] Zhang M, Arendshorst MG, Stevens RJAM. Large eddy simulations of the effect of vertical staggering in large wind farms. *Wind Energy* 2019;22(2):189–204.
- [39] Wu Y, Liao T, Chen C, Lin C, Chen P. Power output efficiency in large wind farms with different hub heights and configurations. *Renew Energy* 2019;132:941–9.
- [40] Liu Y. The effect of vertical arrangement on performance and wake characteristics of two tandem offshore wind turbines under various operating conditions. *Energy Conv Manag* 2023;278:116743.
- [41] Kirchner-Bossi N, Porté-Agel F. Wind farm layout and unconstrained hub height optimization using genetic algorithms applied to different power densities. *J Phys: Conf Ser* 2022;2265:042049.
- [42] Modvion. RES and Modvion enter a new collaboration to bring wooden towers to future wind parks. <https://modvion.com/news/res-and-modvion-enter-a-new-collaboration-to-bring-wooden-towers-to-future-wind-parks/>; 2022 [accessed 11 October 2022].
- [43] Cheng Z, Madsen HA, Gao Z, Moan T. Effect of the number of blades on the dynamics of floating straight-bladed vertical axis wind turbines. *Renew Energy* 2017;101:1285–98.
- [44] Cheng Z, Madsen HA, Chai W, Gao Z, Moan T. A comparison of extreme structural responses and fatigue damage of semi-submersible type floating horizontal and vertical axis wind turbines. *Renew Energy* 2017;108:207–19.
- [45] Lee CF, Cheng Z, Ong MC, Wang K. Extreme response analysis of a floating vertical axis wind turbine based on modified environmental contour method. *Ocean Eng* 2023;270:113459.
- [46] CD-adapco. STAR-CCM+ User Guide Version 13.04. New York, NY, USA: CD-adapco; 2018.
- [47] Rezaieha A, Montazeri H, Blocken B. On the accuracy of turbulence models for CFD simulations of vertical axis wind turbines. *Energy* 2019;180:838–57.
- [48] Su J, Chen Y, Han Z, Zhou D, Bao Y, Zhao Y. Investigation of V-shaped blade for the performance improvement of vertical axis wind turbines. *Appl Energy* 2020;260:114326.
- [49] Miao W, Li C, Yang J, Xie X. Numerical investigation of the yawed wake and its effects on the downstream wind turbine. *J Renew Sustain Energy* 2016;8(3):033303.
- [50] Fu S, Li Z, Zhu W, Han X, Liang X, Yang H, et al. Study on aerodynamic performance and wake characteristics of a floating offshore wind turbine under pitch motion. *Renew Energy* 2023;205:317–25.
- [51] Blocken B. LES over RANS in building simulation for outdoor and indoor applications: a foregone conclusion? *Build Simul* 2018;11(5):821–70.
- [52] Zhang L, Li Y, Xu W, Gao Z, Fang L, Li R, et al. Systematic analysis of performance and cost of two floating offshore wind turbines with significant interactions. *Appl Energy* 2022;321:119341.
- [53] Rezaieha A, Montazeri H, Blocken B. CFD analysis of dynamic stall on vertical axis wind turbines using scale-adaptive simulation (SAS): comparison against URANS and hybrid RANS/LES. *Energy Conv Manag* 2019;196:1282–98.
- [54] Zou Y, Zhao X, Chen Q. Comparison of STAR-CCM+ and ANSYS fluent for simulating indoor airflows. *Build Simul* 2018;11:165–74.
- [55] Tu Y, Zhang K, Han Z, Zhou D, Bilgen O. Aerodynamic characterization of two tandem wind turbines under yaw misalignment control using actuator line model. *Ocean Eng* 2023;281:114992.
- [56] Onel HC, Tuncer IH. Investigation of wind turbine wakes and wake recovery in a tandem configuration using actuator line model with LES. *Comput Fluids* 2021;220:104872.
- [57] IEC. International standard 61400–3–1, Wind energy generation systems - Part 3–1: Design requirements for fixed offshore wind turbines. 2019.
- [58] Kuang L, Zhang R, Su J, Shao Y, Zhang K, Chen Y, et al. Systematic investigation of effect of rotor solidity on vertical-axis wind turbines: power performance and aerodynamics analysis. *J Wind Eng Ind Aerodyn* 2023;233:105284.
- [59] Rezaieha A, Kalkman J, Blocken B. CFD simulation of a vertical axis wind turbine operating at a moderate tip speed ratio: guidelines for minimum domain size and azimuthal increment. *Renew Energy* 2017;107:373–85.
- [60] Baldazzi F, Bianchini A, Maleci R, Ferrari G, Ferrari L. Critical issues in the CFD simulation of Darrieus wind turbines. *Renew Energy* 2016;85:419–35.
- [61] Wu Y, Lin C, Chang T. Effects of inflow turbulence intensity and turbine arrangements on the power generation efficiency of large wind farms. *Wind Energy* 2020;23(7):1640–55.
- [62] Cheng Z, Madsen HA, Gao Z, Moan T. A fully coupled method for numerical modeling and dynamic analysis of floating vertical axis wind turbines. *Renew Energy* 2017;107:604–19.
- [63] Shaaban S, Albatal A, Mohamed MH. Optimization of H-rotor Darrieus turbines' mutual interaction in staggered arrangements. *Renew Energy* 2018;125:87–99.
- [64] Sahebzadeh S, Rezaieha A, Montazeri H. Towards optimal layout design of vertical-axis wind-turbine farms: double rotor arrangements. *Energy Conv Manag* 2020;226:113527.
- [65] Peng H, Lam H, Lee C. Investigation into the wake aerodynamics of a five-straight-bladed vertical axis wind turbine by wind tunnel tests. *J Wind Eng Ind Aerodyn* 2016;155:23–35.
- [66] Borg M, Manuel L, Collu M, Liu J. Long-term global performance analysis of a vertical-axis wind turbine supported on a semi-submersible floating platform. In: Proceedings of the ASME 2015 34th International Conference on Ocean, Offshore and Arctic Engineering. 9; 2015. V009T09A066.
- [67] Hand B, Cashman A. Conceptual design of a large-scale floating offshore vertical axis wind turbine. *Energy Procedia* 2017;142:83–8.
- [68] Araya DB, Colonius T, Dabiri JO. Transition to bluff-body dynamics in the wake of vertical-axis wind turbines. *J Fluid Mech* 2017;813:346–81.
- [69] Chamorro LP, Porté-Agel F. Effects of thermal stability and incoming boundary-layer flow characteristics on wind-turbine wakes: a wind-tunnel study. *Boundary-Layer Meteorol* 2010;136:515–33.
- [70] Rolin VFC, Porté-Agel F. Experimental investigation of vertical-axis wind-turbine wakes in boundary layer flow. *Renew Energy* 2018;118:1–13.
- [71] Araya DB, Dabiri JO. Vertical axis wind turbine in a falling soap film. *Phys Fluids* 2015;27(9):091108.
- [72] Swanson WM. The Magnus effect: a summary of investigations to date. *J Basic Eng* 1961;83(3):461–70.
- [73] Taguchi G. Introduction to quality engineering: Designing quality into products and processes. Asian Productivity Organization; 1986.
- [74] Chen B, Du J, Yao Y. Power prediction formula for blade design and optimization of dual Darrieus wind turbines based on Taguchi method and genetic expression programming model. *Renew Energy* 2022;192:583–605.

- [75] Chen W, Chen C, Huang C, Hwang C. Power output analysis and optimization of two straight-bladed vertical-axis wind turbines. *Appl Energy* 2017;185:223–32.
- [76] Wang Z, Wang Y, Zhuang M. Improvement of the aerodynamic performance of vertical axis wind turbines with leading-edge serrations and helical blades using CFD and Taguchi method. *Energy Conv Manag* 2018;177:107–21.
- [77] Chen W, Wang J, Chang M, Mutuku JK, Hoang AT. Efficiency improvement of a vertical-axis wind turbine using a deflector optimized by Taguchi approach with modified additive method. *Energy Conv Manag* 2021;245:114609.
- [78] Peng H, Liu M, Liu H, Lin K. Optimization of twin vertical axis wind turbines through large eddy simulations and Taguchi method. *Energy* 2022;240:122560.
- [79] Peng H, Zhong B, Hu G, Liu H. Optimization analysis of straight-bladed vertical axis wind turbines in turbulent environments by wind tunnel testing. *Energy Conv Manag* 2022;257:115411.
- [80] Vaghela PA, Prajapati JM. Hybridization of Taguchi and genetic algorithm to minimize iteration for optimization of solution. *MethodsX* 2019;6:230–8.
- [81] Chen J, Chen L, Xu H, Yang H, Ye C, Liu D. Performance improvement of a vertical axis wind turbine by comprehensive assessment of an airfoil family. *Energy* 2016;114:318–31.
- [82] Phadke MS. Quality engineering using robust design. Prentice Hall PTR; 1995.
- [83] Peng H, Lam F. Turbulence effects on the wake characteristics and aerodynamic performance of a straight-bladed vertical axis wind turbine by wind tunnel tests and large eddy simulations. *Energy* 2016;109:557–68.